Redox Biology 17 (2018) 323–337

Contents lists available at ScienceDirect

Redox Biology

journal homepage: www.elsevier.com/locate/redox

Brain ischemic preconditioning protects against ischemic injury and preserves the blood-brain barrier *via* oxidative signaling and Nrf2 activation

Tuo Yang[a], Yang Sun[a], Leilei Mao[a,b], Meijuan Zhang[a,c], Qianqian Li[a], Lili Zhang[a], Yejie Shi[a], Rehana K. Leak[d], Jun Chen[a,e], Feng Zhang[a,b,*]

[a] Department of Neurology, Pittsburgh Institute of Brain Disorders and Recovery, University of Pittsburgh, Pittsburgh, PA, USA
[b] Department of Neurology and Key Laboratory of Cerebral Microcirculation, University of Shandong, Affiliated Hospital of Taishan Medical College, Tai'an, Shandong, China
[c] Department of Neurology, Affiliated Drum Tower Hospital of Nanjing University Medical School, Nanjing, Jiangsu, China
[d] Graduate School of Pharmaceutical Sciences, Duquesne University, Pittsburgh, PA, USA
[e] Geriatric Research, Educational and Clinical Center, Veterans Affairs Pittsburgh Health Care System, Pittsburgh, PA, USA

ARTICLE INFO

Keywords:
Stroke
Neuroprotection
Ischemic tolerance
Electrophile
Lipid peroxidation
VE-cadherin
Conditioning

ABSTRACT

Brain ischemic preconditioning (IPC) with mild ischemic episodes is well known to protect the brain against subsequent ischemic challenges. However, the underlying mechanisms are poorly understood. Here we demonstrate the critical role of the master redox transcription factor, nuclear factor (erythroid-derived 2)-like 2 (Nrf2), in IPC-mediated neuroprotection and blood-brain barrier (BBB) preservation. We report that IPC causes generation of endogenous lipid electrophiles, including 4-hydroxy-2-nonenal (4-HNE), which release Nrf2 from inhibition by Keap1 (*via* Keap1-C288) and inhibition by glycogen synthase kinase 3β (*via* GSK3β-C199). Nrf2 then induces expression of its target genes, including a new target, cadherin 5, a key component of adherens junctions of the BBB. These effects culminate in mitigation of BBB leakage and of neurological deficits after stroke. Collectively, these studies are the first to demonstrate that IPC protects the BBB against ischemic injury by generation of endogenous electrophiles and activation of the Nrf2 pathway through inhibition of Keap1- and GSK3β-dependent Nrf2 degradation.

1. Introduction

Stroke is a leading cause of long-term disability and death [10]. Although a number of preclinical studies suggest that sublethal, short-duration ischemic episodes induce ischemic tolerance against subsequent longer-duration ischemia [11,27,58], the clinical translation of ischemic preconditioning (IPC) has achieved mixed results [14,39]. One explanation for the lack of clinical translation may be the neurocentric approach to protection in most preclinical studies, which do not always ensure the preservation of non-neuronal cells, such as the components of the blood-brain barrier (BBB). BBB breakdown after stroke allows infiltration of inflammatory factors and immune cells, and produces detrimental clinical consequences, such as brain edema and hemorrhagic transformation [37]. The integrity of tight junctions (TJs) and adherens junctions (AJs) is critical for BBB integrity [17], and, therefore, both are potential targets of IPC-mediated protection. Although IPC has been reported to protect the BBB by enhancing angiogenesis and TJ expression and mitigating inflammation [36,52,70], the details of the molecular mechanisms remain unknown.

The classic view of IPC involves two temporal windows of tolerance—rapid and delayed preconditioning. Rapid tolerance unfolds within minutes of the preconditioning stimulus, whereas delayed tolerance emerges within hours to days [11,43] and confers more robust neuroprotection [58]. Recent evidence also supports the existence of a third window lasting as long as 8 weeks, which can be elicited by repetitive hypoxia, but not ischemia, perhaps by epigenetic regulation [60]. For IPC-mediated delayed tolerance, mild oxidative stress and *de novo* protein synthesis are required [5,40,54], as is upregulation of a panel of phase II enzymes [12,21,53], which possess electrophile response elements (EpRE) in their promoters [20]. EpRE is the binding site for nuclear factor (erythroid-derived 2)-like 2 (Nrf2), a master switch that controls redox equilibrium [25,71]. Under normal conditions, Nrf2 is degraded by the proteasome shortly after synthesis by two independent routes—a canonical route mediated by Kelch-like ECH-associated protein 1 (Keap1) [26], and a non-canonical route mediated by glycogen synthase kinase 3β (GSK3β) [8,44].

The mechanism whereby IPC leads to Nrf2 activation is poorly understood. Among ten categories of Nrf2 inducers [21], the only

* Corresponding author at: Department of Neurology, Pittsburgh Institute of Brain Disorders and Recovery, University of Pittsburgh, Pittsburgh, PA, USA.
E-mail address: zhanfx2@upmc.edu (F. Zhang).

https://doi.org/10.1016/j.redox.2018.05.001
Received 18 February 2018; Received in revised form 23 April 2018; Accepted 3 May 2018
Available online 06 May 2018

endogenous inducers are the Michael reaction acceptors, also known as electrophiles. The predominant electrophiles in cellular systems are the end products of lipid peroxidation, including 4-hydroxy-nonenal (4-HNE) from omega-6 fatty acids and 4-hydroxy-hexenal (4-HHE) from omega-3 fatty acids [16,72]. These electrophiles react readily with Keap1 cysteine thiol groups and play an important role in Nrf2 signaling [32,45]. Given these collective observations, we hypothesized that IPC leads to the generation of a labile pool of lipid electrophiles, including 4-HNE and 4-HHE, which inhibit both Keap1 and GSK3β-dependent degradation of Nrf2, and result in the induction of Nrf2-dependent cytoprotective genes.

In the present study, we report that IPC confers brain protection against ischemic injury and preserves the BBB. We also demonstrate the key role of Nrf2 in IPC-mediated protection and the mechanism of activation of the Nrf2 pathway by lipid electrophiles. In both cellular and animal models, IPC reinforced the BBB along with Nrf2-dependent preservation of endothelial survival and junction proteins. Finally, at the molecular level, we identified critical residues in Keap1 and GSK3β for the inhibition of Nrf2 degradation by lipid electrophiles.

2. Materials and methods

2.1. Animals

All animal experiments were approved by the University of Pittsburgh Institutional Animal Care and Use Committee (IACUC) and carried out in accordance with Stroke Treatment and Academic Roundtable (STAIR) guidelines and the *National Institutes of Health (NIH) Guide for the Care and Use of Laboratory Animals*. This manuscript was written in accordance with ARRIVE guidelines.

Adult male and female C57BL/6 wildtype and Nrf2 knockout (KO) mice were purchased from The Jackson Laboratory (Bar Harbor, ME). All animals were housed in a 12:12 h light-dark cycle at 22–24 °C, with ad libitum access to rodent chow and water. Mice were randomly assigned to experimental groups with a lottery-drawing box. All outcome assessments, including evaluation of ischemic infarction, neurobehavioral performance, and gel analyses were performed by investigators blinded to group assignments. Animal numbers and mortality are listed in Supplementary Table 1.

2.2. Drug administration

For intracerebral ventricle (ICV) injections, mice were anesthetized with 1.5% isoflurane and placed in a stereotaxic frame (Kopf, Tujunga, CA). A midline incision was made over the skull and a burr hole was drilled in the skull. A Hamilton syringe was then lowered into the ventricular compartment with the following coordinates from Bregma: anteroposterior, 0.6 mm; lateral, 1.1 mm; and ventral, 2.2 mm. A total of 5 μL of drug or vehicle was injected. For N-acetylcysteine (NAC) injections, 5 μL of 50 mM NAC in saline was injected 1 h after IPC. For 4-HNE injections, 5 μL of 1.5, 3, 6, or 16 μg of 4-HNE in saline was injected, and cortical tissues were collected 24 h later. The injection lasted for 10 min and was controlled by an UltraMicroPump (World Precision Instruments, Sarasota, FL). The syringe was left in place for an additional 5 min to prevent diffusion up the needle track during withdrawal.

2.3. Middle cerebral artery occlusion (MCAO)

All mice underwent MCAO on the left side for 12 min to induce IPC [59] and 60 min to induce stroke [69,72]. This was followed by reperfusion for the indicated durations. The interval between IPC and stroke was 3 days. MCAO was performed with standard, previously published procedures [69,72]. In brief, mice were anesthetized with 1.5% isoflurane in a 30% O_2/70% N_2O mixture under spontaneous breathing, and rectal temperature was maintained at 37.0 ± 0.5 °C with a temperature-regulated heating pad throughout the surgery. Mean arterial blood pressure was monitored with a tail cuff. Using a surgical microscope, the left external, internal, and common carotid arteries were exposed through a midline neck incision. After coagulating and cutting of the branches of the external carotid arteries, an 8-0 monofilament nylon suture with a silicone coat was inserted in the lumen of the external carotid artery and advanced to the origin of the middle cerebral artery *via* the internal carotid artery.

As dictated by STAIR guidelines, the success of MCAO was confirmed by the measurement of regional cortical cerebral blood flow (rCBF), examination of neurological dysfunction, and the formation of the infarct, as described below. Neurological dysfunction was assessed in all mice once they recovered fully from anesthesia, and the measurements of rCBF and infarct volumes were performed in randomly selected mice, as described below. Mice were excluded from the study if their rCBF failed to fall below 40% of baseline or they showed no neurological deficits in stroke groups after recovery from anesthesia.

rCBF was monitored using Laser speckle contrast imaging, as described previously [51,57]. Briefly, a midline incision was made over the mouse skull, and a charge-coupled device camera (PeriCam PSI System; Perimed Inc., Ardmore, PA) was placed 10 cm above the head. The intact skull surface was illuminated by a laser diode to allow laser penetration through the brain in a diffuse manner. Two-dimensional microcirculation images were obtained 5 min before MCAO, 5 min after MCAO, and 10 min after the onset of reperfusion, including IPC intervals.

During anesthesia and surgery, physiological parameters, including core body temperature and blood pressure, were monitored (Supplementary Table 2). Rectal temperature was monitored and maintained in the normal range using a mouse rectal probe connected to a TCAT-2LV controller (Physitemp, Clifton, NJ). Blood pressure was measured using a mouse tail-cuff and a PowerLab system (ADInstruments, Colorado Springs, CO), as described previously [69,72].

2.4. Assessment of stroke outcome

Stroke outcome was assessed by neurological scoring, TTC staining, and behavioral tests

2.4.1. Neurological scoring and TTC staining

Neurobehavioral and histological studies were performed to evaluate ischemic outcomes by blinded observers. For the acute studies (48 h), neurologic dysfunction was scored at indicated time points after MCAO using the 5-point method [73], with 0 being the least dysfunction and 4 the worst dysfunction. Mice were then sacrificed and brains removed and sliced into 7 coronal sections each 1 mm thick. Sections were then stained with 2% 2,3,5-triphenyltetrazolium chloride (TTC) to determine infarct volumes [72,73]. Infarct volumes were measured blinded using NIH Image J software (Bethesda, MD).

2.4.2. Behavioral tests

To evaluate long-term sensorimotor functions, the Rotarod test (IITC Life Science Inc., Woodland Hills, CA) and adhesive removal test were performed up to 7 days after stroke [56,57,72]. The rotarod test evaluates sensorimotor coordination and balance. First, mice were trained for three days before surgery. After the mice were placed on the rods (diameter 3 cm), the rods began to rotate and accelerate to 25 rpm within 300 s. The maximal length of each trial was 300 s. Results are presented as the duration that the mice were able to remain on the rods. If the mice could remain on the rod for the entire 300 s, the rotations were stopped; if the mice fell from the rods before 300 s, the drop was recorded automatically by magnetic switches [57,72]. The adhesive removal test also evaluates sensorimotor function. Two adhesive paper patches (3 × 4 mm) were securely attached to the distal radial region of each forelimb. The time to remove each patch from the forelimbs was recorded [6]. Mice were trained once daily for 5 days before surgery.

Three trials were completed per testing day, with a minimal interval of 5 min between consecutive trials.

2.5. Electrophoretic mobility shift assay (EMSA)

Brain tissues were harvested at the indicated time points after IPC in mice. Whole cell lysates were prepared, and nuclear and cytoplasmic fractions were extracted using an NE-PER nuclear and cytoplasmic extraction kit (ThermoFisher Scientific, Pittsburgh, PA) according to the manufacturer's instructions [72]. EMSA was performed to detect the DNA binding activity of Nrf2 in nuclear extracts, using a Gel-Shift kit (Affymetrix, Santa Clara, CA) [72]. In brief, the Nrf2 consensus oligonucleotide (5′-GCTCTTCCGGTGCTCTTCCGGT-3′) was labeled with biotin. The DNA-protein-binding reaction was performed according to the manufacturer's instructions. The reaction mixture was then subjected to electrophoresis. The specificity of EpRE-binding activity of Nrf2 was determined by performing competition assays, in which 1-fold and 50-fold molar excess of cold probes were used as competitors.

2.6. In vivo BBB permeability assay

BBB permeability was determined by measurements of endogenous IgG leakage [51]. Two days after stroke, the brains were harvested and paraffin sections were collected. Sections were blocked for 1 h, followed by incubation with biotinylated horse anti-mouse IgG antibodies (1:500; Vector Laboratories, Burlingame, CA). Sections were then incubated with streptavidin-488 (Vectastain Elite ABC; Vector Laboratories, Burlingame, CA) for one hour. Images were obtained and IgG leakage volume and staining intensity were calculated on six equally spaced sections encompassing the MCA territory.

2.7. PCR array

To detect the induction of oxidative stress genes by IPC, we performed the Oxidative Stress PCR Array on brain tissue. In brief, 6 h after IPC, brain tissues in the MCA region were harvested and stored in RNase-free tubes. The RNA was extracted and purified, and RNA quantity and purity was determined by spectrophotometry. Next, RNA was converted to first-strand cDNA using the RT2 First Strand Kit (Qiagen, Germantown, MD). The cDNA was then added to the RT2 Master Mix and RNase-free water, and this mixture was loaded into the wells of the PCR Array plates for real-time PCR. Data were analyzed using PCR Array Data Analysis Software (Qiagen).

2.8. Western blots and western dot blots

Brain tissues were harvested at the indicated time points after ischemia or after 4-HHE and HNE treatments (n = 4 per experimental condition). Whole cell lysates were prepared and in some experiments, nuclear and cytoplasmic fractions were extracted as described above. Protein concentrations were determined by the bicinchoninic acid assay (Bio-Rad, Hercules, CA). Equal amounts of protein samples were loaded onto acrylamide gels and subjected to electrophoresis, followed by transfer to polyvinylidene difluoride (PVDF) membranes (Bio-Rad). PVDF membranes were then blocked with 5% non-fat milk, and probed with antibodies recognizing hemo oxygenase-1 (HO-1, 1:1000, Enzo Life Science, Farmingdale, NY), Nrf2 (1:1000, Abcam, Cambridge, MA), glutamate-cysteine ligase modifier subunit (GCLM, 1:1000, Abcam), β-actin (1:3000, Sigma-Aldrich, St. Louis, MO), FLAG (1:1000, Cell Signaling Technology, Danvers, MA), cadherin 5 (CDH5, 1:1000, Abcam), claudin 5 (1:1000, Abcam), Akt (1:1000, Cell Signaling Technology), phosphorylated Akt (p-Akt, S473, 1:1000, Cell Signaling Technology), GSK3β (1:1000, Cell Signaling Technology), phosphorylated GSK3β (p-GSK3β, S9, 1:1000, Cell Signaling Technology), human influenza hemagglutinin (HA, 1:1000, Cell Signaling Technology) or lamin B1 (1:1000, Cell Signaling Technology). After incubation in secondary antibodies (Santa Cruz, Santa Cruz, CA) for 1 h, the membranes were incubated with ECL substrates (Pierce, ThermoFisher Scientific) and developed with X-ray film. ImageJ software was used for gel analyses.

For the Western dot blot assays, proteins were extracted from the brain tissues or cultured cells, and equivalent amounts of proteins were loaded directly onto PVDF membranes using a Bio-Dot Microfiltration apparatus (Bio-Rad, Hercules, CA). Anti-4-HNE (1 μg/mL, R&D, Minneapolis, MN), or anti-Tubulin (1:2000, Abcam, Cambridge, MA) was used as the primary antibody. The remaining procedures were the same as for the Western blots.

2.9. Immunohistochemistry

Mice were sacrificed 2 days after MCAO. Following perfusion with normal saline and fixation with 4% paraformaldehyde, paraffin-embedded brain sections were cut at 5-μm thickness in the coronal plane. Primary antibodies recognizing HO-1 (1:400, Enzo Life Science), NeuN (1:200, Abcam), CD31 (1:200, BD Biosciences, San Jose, CA), glial fibrillary acidic protein (GFAP, 1:500, ThermoFisher Scientific), and ionized calcium binding adapter molecule-1 (Iba-1, 1:1000, Wako Chemicals, Wako, Japan) were applied. After washes in buffer and incubations with fluorophore-conjugated secondary antibodies, brain sections were coverslipped and images were captured using a confocal microscope (Olympus Fluoview FV1000, Center Valley, PA, USA).

After treatments, primary cells were fixed for 10 min, and incubated with primary antibody against CDH5 (1:200, Abcam) followed by secondary antibody. DAPI was applied to counterstain the nucleus. Images were then obtained using a confocal microscope.

2.10. Primary cell cultures and Nrf2 knockdown

Primary mouse brain microvascular endothelial cells (MBMECs) were purchased from Cell Biologics (Chicago, IL, USA). Only passages 3–8 were used. To knock down Nrf2 in MBMECs, Nrf2-shRNA and scramble-shRNA (Sc-shRNA) lentiviral particles were added to cells together with 8 μg/mL polybrene (Santa Cruz Biotechnology) for 16 h. The virus-containing culture media were then replaced with fresh growth media. Experiments were performed 72–96 h after transduction [51].

Primary astrocytes were purified as previously described [49]. In brief, whole brains were dissected from neonatal pups and cortices were removed. Mixed cells were seeded and maintained in glial cell culture media (Dulbecco's Modified Eagle Medium/F12 containing L-glutamine, Minimum Essential Medium, nonessential amino acids, sodium pyruvate, penicillin/streptomycin, and fetal bovine serum, all from Gibco). After 7–10 days, a confluent monolayer of cells was formed. Cells were then agitated to remove microglia and oligodendrocytes. The remaining, adherent astrocyte-rich monolayer was then detached with trypsin and plated in DMEM with 10% FBS. After 3–4 passages, astrocyte cell purity reached 98%, as measured by GFAP expression.

Primary cultures of cortical neurons were dissected from E17-19 fetal rats and maintained in Neurobasal medium supplemented with B27 (Gibco, ThermoFisher Scientific, Pittsburgh, PA), as previously described [69,72]. Experiments were performed 10–14 days after seeding.

2.11. Oxygen-glucose deprivation (OGD) and cell death/viability

OGD was used to mimic *in vitro* ischemia with standard, previously published procedures [69]. For MBMECs and MBMEC/astrocyte co-cultures, 16 h lethal OGD was introduced after 4 h OGD as the preconditioning (PC) stimulus, with an 18 h interval between PC and lethal OGD [51]. Cells were incubated with 10 μM 4-HNE for the indicated durations. For lentiviral infected cells, 10 h lethal OGD was introduced, and 2.5 h OGD was set as the PC stimulus.

The Live/Dead cell viability assay was performed as previously described [72], according to the manufacturer's instructions (Molecular Probes, Eugene, OR). In this assay, red dots (fluorescent ethidium homodimer-1) represent dead cells with compromised membranes and green dots (fluorescent membrane-permeant calcein AM) represent live cells. For cell counting, three random fields were captured per well by a blinded observer. Four to six wells per condition per experiment were selected, and the experiments were repeated on three independent occasions.

Extracellular lactate dehydrogenase (LDH) release from damaged cells was measured with an LDH detection kit (Pointe Scientific Inc., Canton, MI). The average LDH released from a total cell lysate in the control group was set as 100%, and all the data were expressed as a relative percentage compared to this value.

2.12. In vitro BBB model and permeability assay

In vitro BBB models were established to measure permeability, as previously described [51]. Transwell inserts (pore size 0.4 μm, Falcon, Corning, NY) were placed into 24-well plates to divide each well into top (luminal) and bottom (abluminal) compartments. This apparatus allows for free passage of nutrients while cellular trafficking across the compartments is blocked. After OGD treatment, FITC-dextran (4 kDa, Sigma-Aldrich, St. Louis, MO) was added into the top compartment at a final concentration of 0.05 mg/mL for the indicated durations, and fluorescence intensity was measured in an aliquot of 50 μL media from the bottom compartment. For the monoculture model, MBMECs were plated into the inserts and incubated until confluence was achieved. For the co-culture model, inserts were reversed, and astrocytes were plated onto the reversed surface for 20 min in the incubator, which is sufficient for astrocyte adherence. Next, inserts were placed into the 24-well plates in the presence of culture media. MBMECs were then plated into the insert.

2.13. CDH5 promoter activity assay

Mouse CDH5 promoter expression plasmids (Chromosome 8+: 104,100,284–104,101,887, translational start site: 104,101,625) with both Gaussia luciferase (GLuc) and secreted alkaline phosphatase (SEAP) reporters were packaged with a third-generation lentiviral system (GeneCopoeia, Rockville, MD) [61]. Briefly, human embryonic kidney (HEK) 293T were grown to 70–80% confluence, and CDH5 promoter plasmids and with lentivirus HIV plasmids were co-transduced. Three days after transduction, supernatants containing lentivirus particles were collected for subsequent experiments.

To assess the role of Nrf2 on MBMEC CDH5 promoter activity, MBMECs were infected by CDH5 promoter expression lentivirus with or without Nrf2/Sc-shRNA expression lentivirus. A Secrete-Pair Dual Luminescence kit (GeneCopoeia) was used to measure GLuc and SEAP luminescence intensities in the supernatants 72 h after transduction. SEAP was set as an internal standard control, and GLuc/SEAP ratios were calculated for each sample. Data were presented as relative to non-transfected controls.

2.14. Keap1 and GSK3β plasmid transfection

HA-tagged GSK3β WT pcDNA3 was a kind gift from Jim Woodgett (Addgene plasmid #14753), and GSK3β S9A and C199A mutations were performed by Biomatik Corporation (Wilmington, DE). Nrf2 pcDNA3 was a kind gift from Yue Xiong (Addgene plasmid #21549). P3xFLAG-tagged WT, C151S, and C288S mouse Keap1 plasmids were kind gifts from Dr. Emilia Kansanen (University of Eastern Finland). All mutations were verified by sequencing. These plasmids were amplified with competent *E. coli* (New England BioLabs, Ipswich, MA) and purified with QIAprep Spin Miniprep Kit (Qiagen).

HEK 293T cells were transfected with Nrf2, FLAG-Keap1 plasmids, or HA-GSK3β plasmids using X-tremeGENE 9 DNA transfection reagent (Roche, Indianapolis, IN) following the manufacturer's instructions. Forty-eight hours after transfection, total cell lysates were harvested with or without 4-HNE stimulation at 30 μM for 2 h.

2.15. Immunoprecipitation (IP)

IP was performed following the instructions of the HA tag IP kit (Pierce, ThermoFisher Scientific) or FLAG tag IP kit (Sigma-Aldrich). In brief, equivalent amounts of total cell lysates extracted from transfected HEK 293T cells were incubated with anti-HA or anti-FLAG resin at 4 °C overnight with end-over-end mixing. After three washes, the resin was eluted with non-reducing sample buffer (ThermoFisher Scientific) and denatured at 100 °C for 5 min prior to standard SDS-page Western blotting.

2.16. Cell-free GSK-3β activity assay

Cell-free GSK-3β activity assays were performed as previously described [34]. In brief, after IP, the HA-resin was washed twice with Tris-buffered saline with 0.1% Tween, followed by one wash with kinase reaction buffer (Cell Signaling Technology). Next, immunoprecipitated GSK3β (WT and mutant) was resuspended in 50 μL kinase reaction buffer in the presence of 1 μg β-catenin (β-Cat, Sigma-Aldrich) as substrate and 0.4 mM ATP (Cell signaling technology). To test the inhibitory effect of electrophiles, 4-HNE was added to the reaction system at the indicated concentrations for 1 h prior to initiation of the activity assay. The kinase reaction was carried out at 37 °C for 30 min under gentle agitation, and terminated by adding 4× reducing sample buffer (Bio-Rad), and denatured by heating at 100 °C for 5 min. The levels of phospho-β-catenin (p-β-Cat, S33/37/T41, Cell Signaling Technology) and total β-catenin (t-β-Cat, Cell Signaling Technology) were analyzed using Western blotting, and the ratios of p-β-Cat/t-β-Cat were calculated to represent GSK3β activity.

2.17. Phosphatase and tensin homolog (PTEN) activity assay

The PTEN activity assay was performed was previously described [50]. For each reaction, 400 ng recombinant PTEN (rPTEN, R&D, Minneapolis, MN) was incubated with 4-HNE or 4-HHE in 50 mM tricine and 100 mM NaCl (pH = 8.0) assay buffer for 30 min at room temperature. The reaction was then ceased by incubation in 2 mM DTT for 30 min. Next, 40 μM phosphatidylinositol-3,4,5-trisphosphate diC8 (Echelon, Salt Lake City, UT) was applied to 25 μL of the PTEN reaction mixture to detect the phosphatase activity of rPTEN at 37 °C. The reaction was stopped 40 min later. BIOMOL Green kit (Enzo Life Science, Farmingdale, NY) was used to measure the released phosphate. Briefly, 25 μL PTEN reaction samples were incubated with 100 μL of BIOMOL Green for 15 min. The phosphate concentration was measured with a microplate reader (Bio-Rad) at 655 nm. All data were presented as picomoles of phosphate per 25 μL reaction.

2.18. Statistical analyses

Results are presented as mean ± SEM, unless indicated otherwise. The difference between means was assessed by the Student's *t*-test (single comparisons) or by Analysis of Variance (ANOVA) followed by *post hoc* Scheffe tests (for multiple comparisons). A p-value ≤ 0.05 was deemed statistically significant.

2.19. Data availability

All relevant data are available within the article and Supplementary files. All other data are available from the corresponding author upon request.

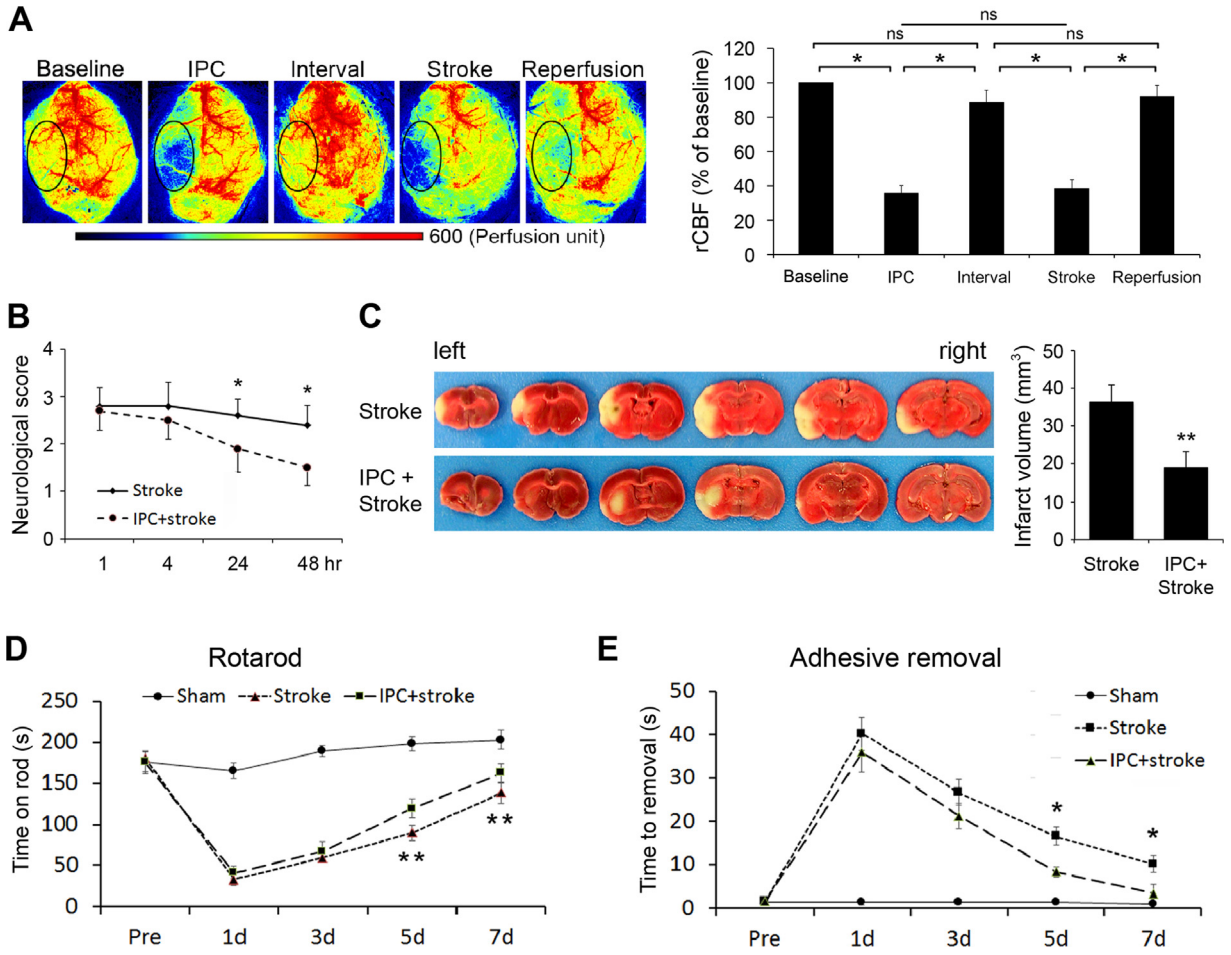

Fig. 1. IPC significantly improves stroke outcomes. IPC was induced in mice by 12-min MCAO and stroke was induced by 60-min MCAO. (A) Representative laser-speckle images and quantitative analyses of rCBF changes, showing successful IPC, stroke, and reperfusion in the left hemisphere. Black ovals indicated the regions of interest. n = 4; ns: not significant; *p < 0.05. (B) Neurological scoring showing that IPC reduced neurological dysfunction. n = 8; *p < 0.05 *vs* Stroke (C) Representative TTC stains and quantification of infarct volumes 48 h after stroke, showing that IPC reduced brain infarction. n = 8, **p < 0.01 *vs* Stroke. (D) Rotarod tests and (E) adhesive removal tests showed that IPC improved sensorimotor dysfunction after stroke. n = 6–8; *p < 0.05, **p < 0.01 *vs* Stroke.

3. Results

3.1. IPC protects mice against ischemic brain injury at the structural and functional levels

IPC was induced in adult male C57BL/6J mice using 12-min MCAO; three days later, stroke was induced by 60-min MCAO, as previously described [58,59,72]. We confirmed that both IPC and stroke reduced rCBF (Fig. 1A). As expected, IPC significantly reduced neurological dysfunction (Fig. 1B) and infarct volume (Fig. 1C) 48 h after stroke, indicating a protective role of IPC. Similar results were evident in female mice (Supplementary Fig. 1). To determine if IPC offers functional neuroprotection, we performed the Rotarod and adhesive removal tests up to 7 days after stroke. As shown in Fig. 1D and E, IPC improved sensorimotor function compared to the Stroke group, as indicated by increased time spent on the rotating rods without falling off and decreased latency to remove the paw adhesives. Taken together, these data confirm that IPC elicited structural and functional protection against ischemic stroke.

3.2. IPC activates the Nrf2 pathway mainly in endothelial cells in vivo

As IPC provides protection by inducing the synthesis of new proteins, we determined which proteins are upregulated by IPC, beginning with Nrf2 target enzymes. First, we extracted cytosolic and nuclear proteins from cortical tissues and verified that IPC causes nuclear translocation of Nrf2, peaking approximately 4 h after IPC (Fig. 2A). EMSA confirmed increased DNA binding of Nrf2 following its nuclear translocation. As shown in Fig. 2B, IPC significantly increased the EpRE binding activity of Nrf2 at 4 and 24 h. This binding was specific, because the competition assay confirmed that adding cold probes inhibited the DNA binding of Nrf2.

To determine if Nrf2 binding to DNA stimulates the transcription of Nrf2-targeted genes, we extracted total mRNA from cortical tissues 6 h after IPC and performed Antioxidant Defense PCR Arrays. As shown in Fig. 2C, IPC significantly increased the transcription of the expected genes, including Ho-1, NAD(P)H dehydrogenase quinone 1 (Nqo-1), glutathione peroxidase 5 (Gpx5), glutamate-cysteine ligase catalytic subunit (Gclc), and Gclm. Western blotting experiments confirmed that HO-1 (Fig. 2D) and GCLM (Fig. 2E) proteins were significantly upregulated in cytosolic extracts. These findings confirm that IPC activates the Nrf2 pathway and upregulates its target enzymes.

Next, we determined in which neural cell type Nrf2 is activated by IPC. HO-1 can serve as a reliable marker of Nrf2 activation, because HO-1 is expressed at low levels under normal conditions but significantly upregulated after Nrf2 activation [69,72]. *In vitro* cultures of rat primary neurons, astrocytes, and endothelial cells (ECs) all exhibited elevation in HO-1 expression in response to 4-HNE, a known Nrf2 activator (Fig. 2F) [72]. However, immunostaining revealed that only CD31-positive ECs presented with prominent Nrf2 activation after

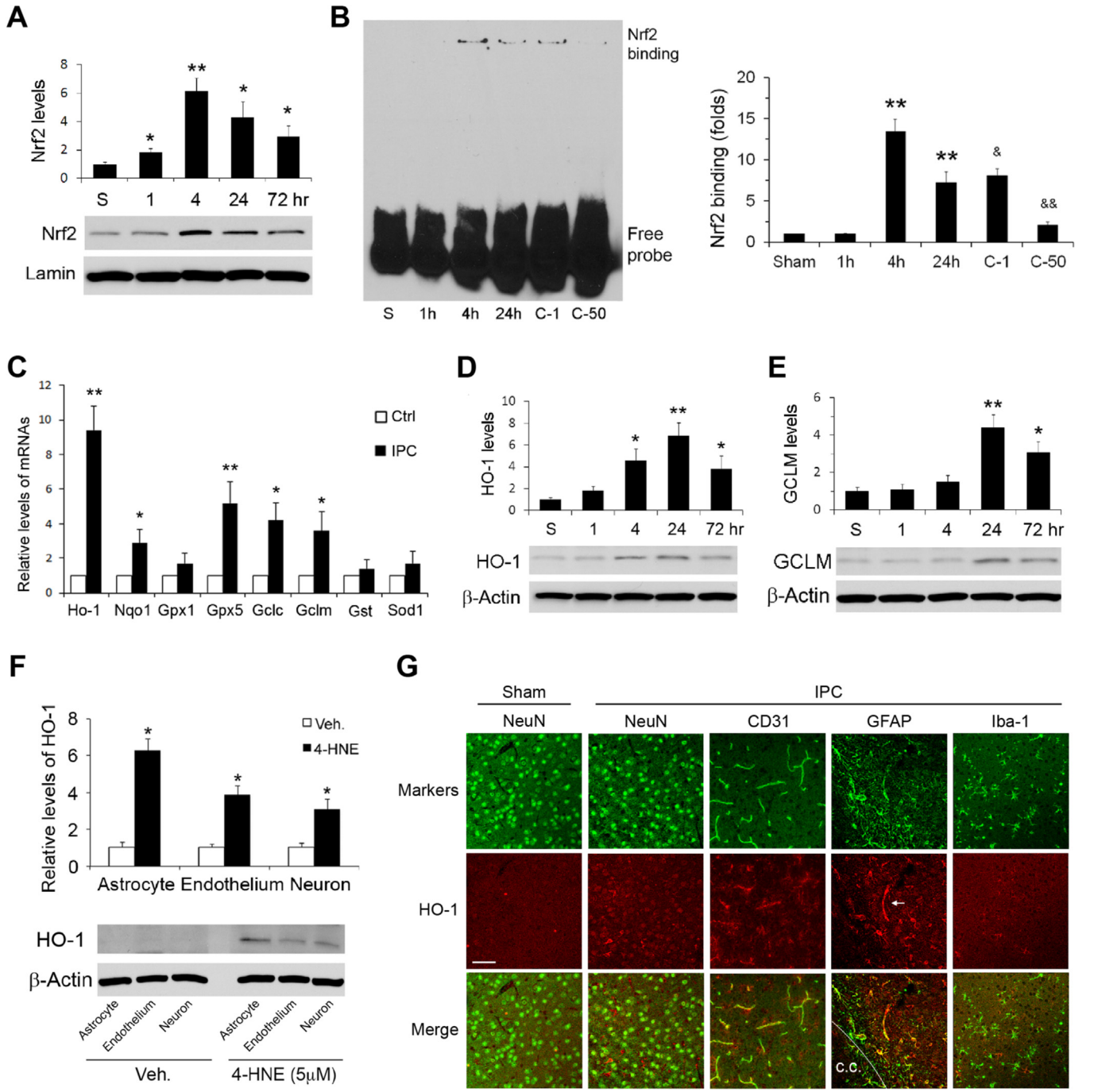

Fig. 2. IPC activates Nrf2 pathway mainly in microvessels. IPC was induced in mice by 12-min MCAO. (A) Representative Western blotting and semi-quantitative analyses of Nrf2 levels within nuclei demonstrated that IPC increased nuclear Nrf2 levels. n = 3; *p < 0.05, **p < 0.01 *vs* Sham (S). (B) Representative EMSA and semi-quantitative analyses showing that IPC increased Nrf2 binding activity. n = 3; **p < 0.01 *vs* Sham and 1-h groups after IPC. The specificity of DNA binding activity of Nrf2 was confirmed by a competition assay, in which 1-fold (C-1) or 50-fold (C-50) excess cold probe was added to the reaction. $^{\&}p < 0.05$ and $^{\&\&}p < 0.01$ *vs* 4-h group. (C) PCR arrays demonstrated that IPC increased the transcription of a panel of phase 2 genes 6 h after IPC. n = 3; *p < 0.05, **p < 0.01 *vs* Ctrl. Western blotting of two representative phase 2 enzymes, (D) HO-1 and (E) GCLM confirmed the PCR results. n = 3, *p < 0.05 and **p < 0.01 *vs* Sham (S). (F) Primary astrocytes, endothelial cells, and neurons all expressed HO-1 after 30 min incubation with 4-HNE (5 μM). n = 3, *p < 0.05 *vs* vehicle. (G) Immunofluorescent staining for HO-1 in the cerebral cortex 48 h after IPC. Robust HO-1 was observed in CD31-positive endothelial cells as well as selected astrocytes associated with microvessels (arrow) near the corpus callosum (c.c.). Scale bar = 50 μm.

IPC *in vivo* (Fig. 2G). HO-1-expressing astrocytes (GFAP-positive) were distributed in tight association with microvessels (arrow) and in a limited region along the corpus callosum. NeuN-positive cortical neurons expressed very weak HO-1, and HO-1 was barely detectable in Iba1-positive microglia in the cortex. Our results therefore suggest that IPC upregulates phase II enzymes after IPC predominantly in microvessels (Fig. 2G).

3.3. Nrf2 plays a key role in IPC-mediated BBB preservation and neuroprotection

As microvessels are the main structural elements of the BBB, we

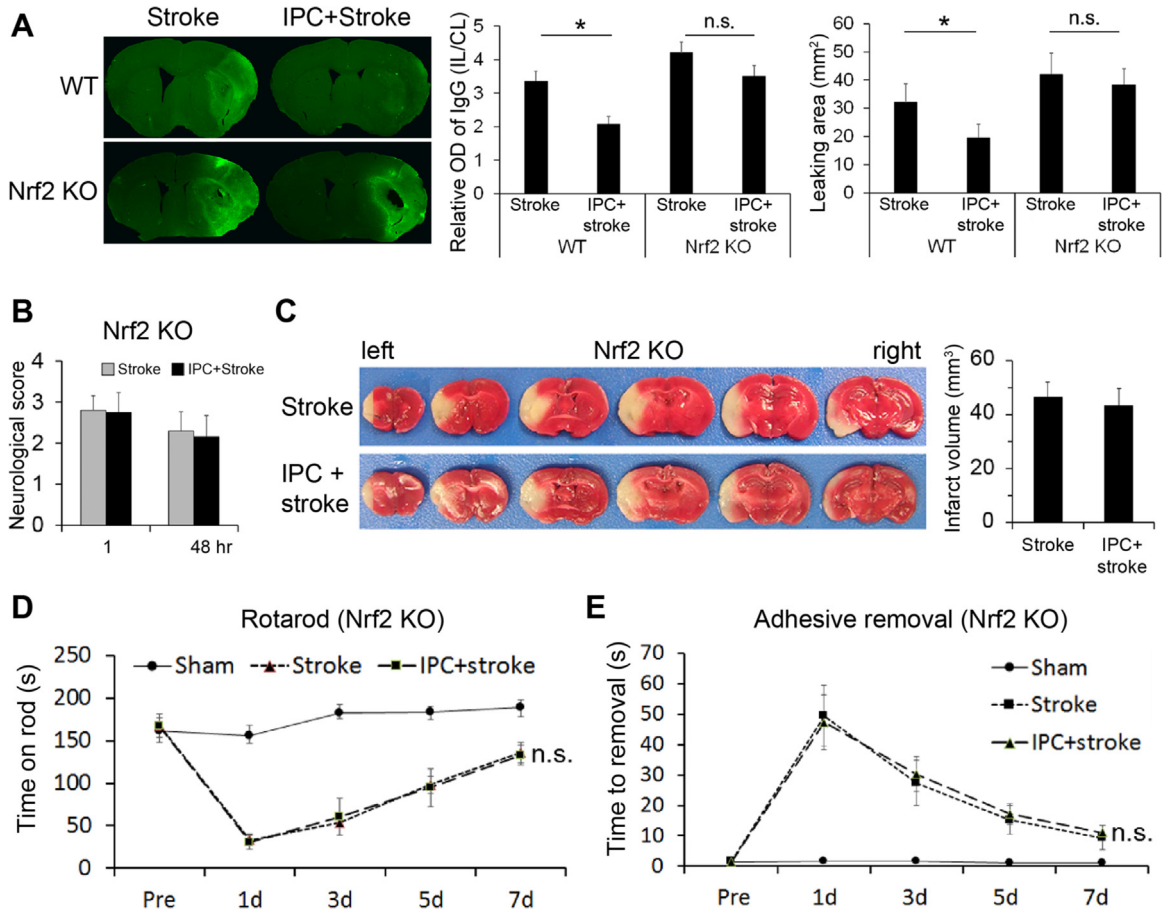

Fig. 3. Key role of Nrf2 in IPC-mediated BBB preservation and neuroprotection. IPC was induced in mice by 12-min MCAO, followed by stroke induction with 60-min MCAO. (A) Representative images of IgG immunostaining in mouse brains 48 h after stroke. Analyses of IgG immunofluorescence intensity and areas with IgG leakage, showing that IPC reduced BBB leakage in WT but not in Nrf2 KO mice. n = 6. *p < 0.05 *vs* Stroke. (B) Neurological score and (C) representative TTC staining and analyses of infarct volumes indicated that IPC failed to protect against ischemic brain injury in Nrf2 KO mice. Data are shown as mean ± SD, n = 7–8, No significant differences were observed between groups. Both (D) Rotarod test and (E) adhesive removal test in Nrf2 KO mice showed that IPC failed to improve stroke-induced sensorimotor deficits. n = 7–8 per group. n.s.: not significant.

examined BBB leakage by applying antibodies against endogenous mouse IgGs to brain sections harvested from preconditioned and control mice two days after stroke. As shown in Fig. 3A, stroke caused substantial IgG penetration from the blood into brain parenchyma, and this leakage was alleviated by IPC. Notably, IPC failed to protect the BBB in Nrf2 KO mice, indicating a critical role of Nrf2 in IPC-mediated BBB protection (Fig. 3A). Consistent with the lack of BBB protection, the absence of Nrf2 expression also completely abolished the protective effects of IPC against neurological deficits (Fig. 3B), brain infarction (Fig. 3C), and sensorimotor impairments (Fig. 3D, E). Collectively, these findings indicate that Nrf2 is essential for BBB preservation and neuroprotection *in vivo*.

3.4. Activation of Nrf2 by lipid electrophiles mediates neuroprotection in IPC

Given the key role of Nrf2 in BBB and brain protection, we then explored the mechanism of Nrf2 activation by IPC. According to Holtzclaw et al., Nrf2 activators fall into one of ten categories [21]. The only Nrf2 activators that can be generated endogenously are Michael reaction acceptors, including lipid electrophiles such as 4-HNE and 4-HHE. As the brain is rich in labile long-chain polyunsaturated fatty acids, it seemed likely that lipid electrophiles are produced after IPC and activate the Nrf2 pathway. We observed a basal level of 4-HNE modified proteins (Fig. 4A) under physiological conditions, consistent with previous reports [72]. The levels of 4-HNE modified proteins increased slightly but significantly after IPC, albeit not as robustly as after stroke (Fig. 4A). These results confirm that IPC causes mild oxidative stress and generates sublethal levels of lipid electrophiles. We also confirmed that ICV 4-HNE delivery dose-dependently increased the levels of HO-1 in the mouse cortex (Fig. 4B). In accordance with the *in vivo* findings, HO-1 expression was also increased in MBMEC cultures in response to PC and 4-HNE in a time-dependent manner (Fig. 4C).

In order to investigate whether electrophiles are critical in IPC-mediated neuroprotection, electrophiles generated by IPC were neutralized by the thiol antioxidant NAC. As shown in Fig. 4D and E, NAC blunted IPC-mediated neuroprotection, confirming the key role of electrophiles in IPC *in vivo*. These collective findings suggest that lipid electrophiles are essential for IPC-mediated brain protection *via* Nrf2 activation. Considering the prominent Nrf2 activation in ECs after IPC (Fig. 2G), and the necessity of Nrf2 in IPC-provided BBB protection (Fig. 3A), we explored the cellular and molecular mechanisms underlying preservation of the BBB by IPC and electrophiles.

3.5. IPC and lipid electrophiles protect against endothelial cell death and preserve BBB integrity by activation of Nrf2

ECs are key elements of the BBB and are highly susceptible to oxidative stress and ischemic injury [13]. Cultures of MBMECs were subjected to OGD, with or without pretreatment with PC or 4-HNE. Live/dead staining and LDH release measurements confirmed that both 4-HNE and PC significantly reduced cell death after OGD (Fig. 5A–C). To

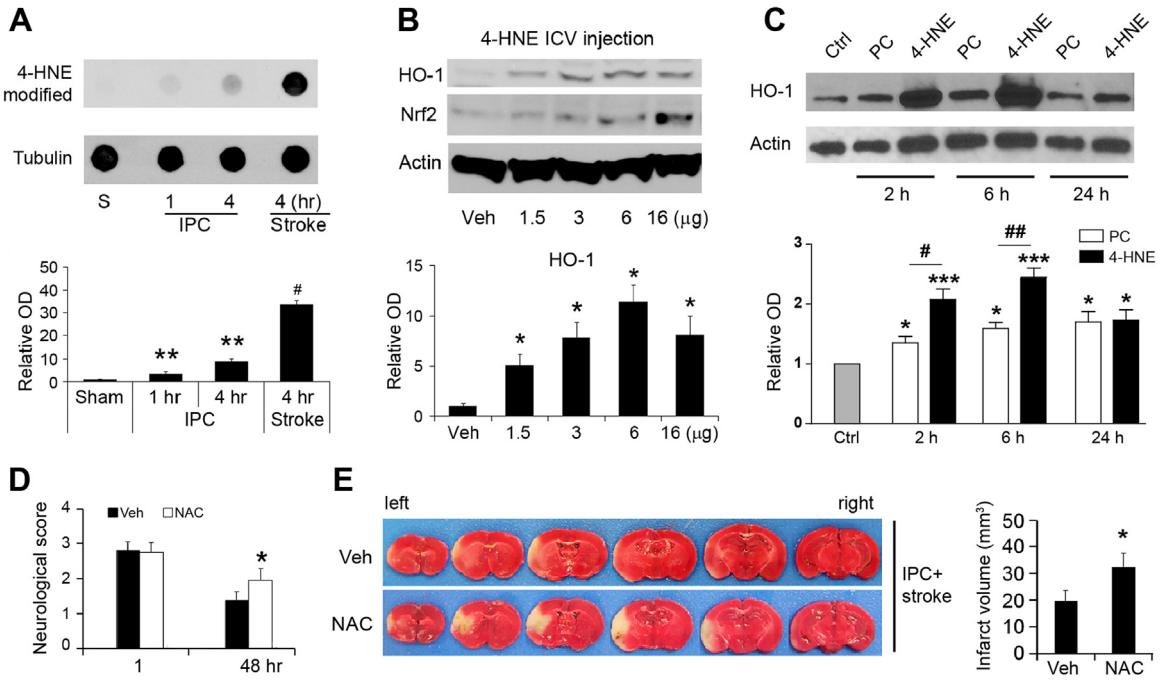

Fig. 4. Lipid electrophiles play a key role in IPC-afforded neuroprotection. IPC was induced by 12-min MCAO followed by stroke induction with 60-min MCAO in mice. PC was induced by 4-h OGD in MBMEC cultures. (A) Representative Western dot blots and semi-quantitative analyses of the levels of 4-HNE modified proteins in mouse brains, showing increased levels of 4-HNE modified proteins after IPC and stroke. n = 4, **p < 0.01 *vs* Sham and #p < 0.01 *vs* IPC. (B) 4-HNE ICV injection increased HO-1 in the brains at 24 h. n = 4, * p < 0.01 *vs* Vehicle. (C) Consistently, both PC and 4-HNE treatment increased HO-1 in MBMECs. n = 3, * p < 0.05 and ***p < 0.001 vs Ctrl, # p < 0.05 and ## p < 0.01. (D) Neurological score and (E) representative TTC stains and analyses of infarct volumes, showing that administration of NAC abolished the protective properties of IPC against stroke. n = 8, *p < 0.05 *vs* Veh.

investigate if PC or 4-HNE preserves *in vitro* BBB integrity, two transwell insert models of the BBB were employed—an MBMEC monoculture model and an MBMEC/astrocyte co-culture model (Fig. 5D). In the monoculture BBB model, both 4-HNE and PC reduced OGD-induced fluorescence dye leakage (Fig. 5E). In the co-culture model, both 4-HNE and PC reduced OGD-induced cellular death (Fig. 5F) and dye leakage (Fig. 5G). It is worth noting that both the LDH release and dye leakage were lower in co-cultures than monocultures after OGD, consistent with a supportive role of astrocytes in protecting the BBB against ischemic injury. These data are also consistent with the observations that IPC induced HO-1 in both endothelial cells and astrocytes *in vivo* (see Fig. 2G).

To determine if these protective effects are Nrf2-dependent, we knocked down Nrf2 in MBMECs using lentiviral particles carrying Nrf2-shRNA and then subjected the MBMECs to PC or 4-HNE followed by 10 h of OGD. As shown in Fig. 5H–J, Nrf2 knockdown compromised the protective effects of PC and 4-HNE, indicating an indispensable role of Nrf2 in EC protection. Taken together, these results suggest that PC and electrophiles prevent EC death and preserve EC integrity in an Nrf2-dependent manner; this mechanism may therefore underlie IPC-mediated BBB protection.

3.6. IPC protects against loss of junction proteins after ischemic injury

Both TJs and adherens junctions (AJs) maintain the integrity of the BBB [17]. Therefore, we examined whether IPC affects the expression of claudin 5, a key TJ protein, and CDH5 (also known as VE-cadherin), a major AJ protein. Mouse brain tissues were harvested at the indicated time points after IPC and subjected to Western blotting (Fig. 6A). As expected, IPC significantly increased the expression of claudin 5 and CDH5 in brain tissues, consistent with a role in BBB reinforcement by IPC. Similarly, PC and 4-HNE also maintained the levels of CDH5 in MBMECs after OGD (Fig. 6B).

The core sequence of EpRE is 5′-nTGACnnnGC-3′, where “n” is any nucleotide [28,66]. We analyzed the mouse CDH5 promoter and identified two potential EpREs (Chromosome 8+: 104,100,284–104,101,887; translational start site = 104,101,625) [15,24]. The first is C*TGAC*CAA*GC*T (from − 377 to − 366) and the second is C*TGAC*CAA*GC*T (from − 126 to − 115). In order to investigate whether Nrf2 can directly upregulate CDH5, we transduced MBMECs with a CDH5 promoter plasmid containing dual luciferase reporters together with Nrf2-shRNA. Compared to Sc-shRNA, Nrf2-shRNA significantly reduced CDH5 promoter luciferase activity (Fig. 6C), indicating that CDH5 may indeed be a target of Nrf2 after IPC.

3.7. Inhibitory effects of electrophiles on Keap1 function

The canonical route for Nrf2 degradation is mediated by Keap1 and Cullin3 (Cul3)-related E3 ligase [32]. To determine if lipid electrophiles activate Nrf2 by inhibiting Keap1 and to pinpoint the sites of electrophile reactions with Keap1 (*e.g.* C151 and C288), we transfected Nrf2 and FLAG-Keap1 plasmids (vector, WT, C151S, C288S or C151S + C288S double mutation) into HEK 293T cells. Cells were then treated with 30 μM 4-HNE for 2 h and Nrf2 and FLAG levels were measured in total cell lysates (Fig. 7A). In WT and C151S-mutants, Nrf2 levels were increased in response to 4-HNE; however, with C288S and C151S + C288S mutations, Nrf2 was constitutively upregulated regardless of the presence or absence of 4-HNE. We also observed significant decreases in FLAG in the C288S group. These findings led us to further explore the protein-protein interactions underlying IPC.

According to a recent “conformation cycling” theory [4], Keap1 binds Nrf2 and guides it to the proteasome under basal conditions; Keap1 then disassociates from Nrf2 and is recycled to bind *de novo* synthesized Nrf2 (Fig. 8A). Failure of binding and failure of dissociation can both lead to Nrf2 transactivation. To elucidate how 4-HNE affects this cycle, similar amounts of FLAG-Keap1 were pulled down from total cell lysates by FLAG-conjugated resin in both reducing

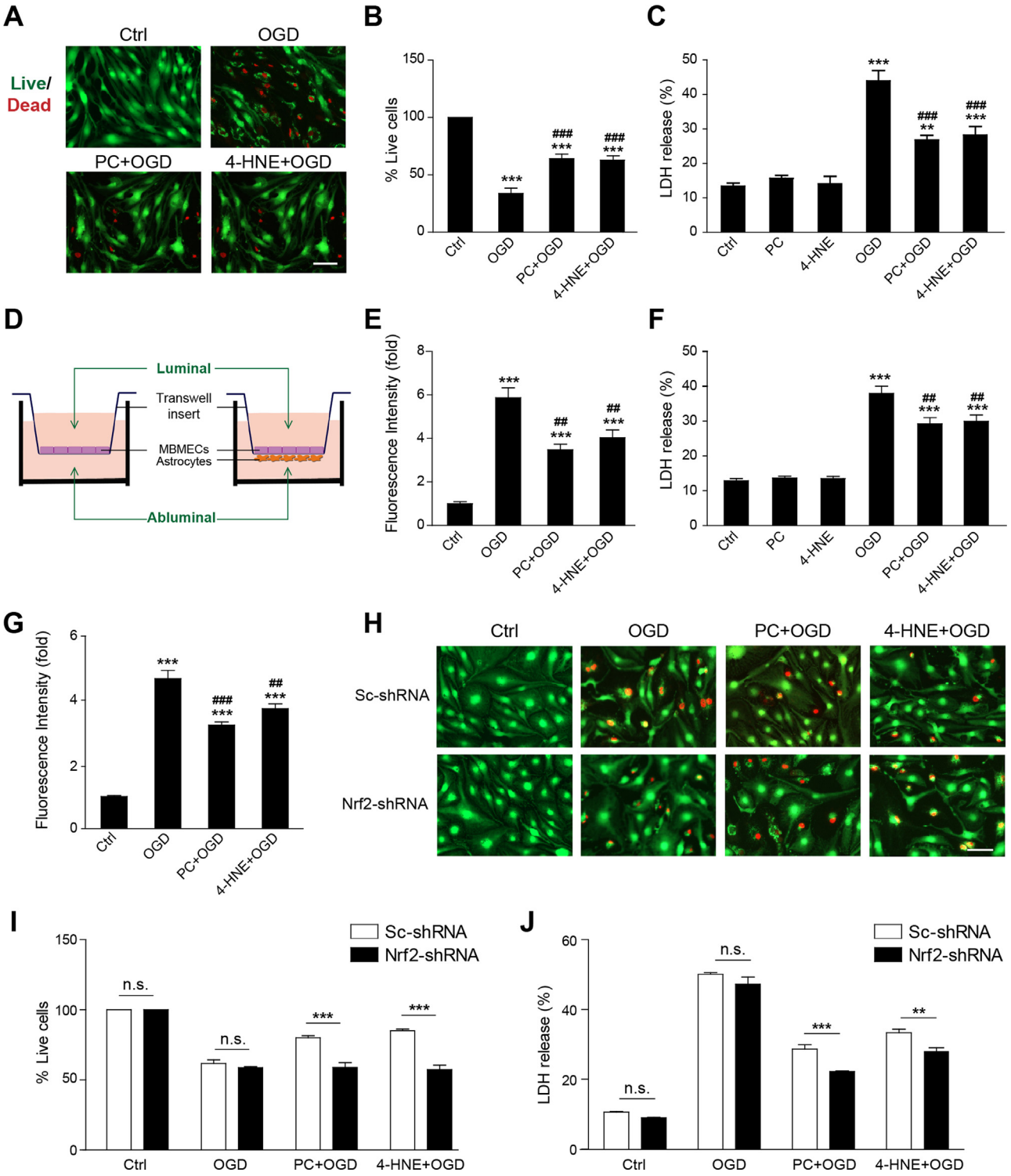

Fig. 5. Lipid electrophiles and PC protect against endothelial death and disintegrity dependent on Nrf2. MBMECs were subjected to lethal OGD after PC or 4-HNE treatment. (A) Live/Dead staining with (B) cell counting and (C) the LDH assay demonstrated increased cell survival and decreased cell death by both PC and 4-HNE. (D) *In vitro* BBB models were created by plating either MBMECs on the luminal side, or MBMECs (luminal side) and astrocytes (abluminal side) on each side. FITC-dextran was added to the luminal compartments, and dextran leakage was evaluated by measuring fluorescent intensities in the abluminal compartments 8 h after OGD. (E) OGD significantly increased dextran leakage in MBMEC cultures, which was partially reversed by both PC and 4-HNE. (F) In MBMEC-astrocyte cocultures, both PC and 4-HNE attenuated OGD-induced cell death, as indicated by the LDH assay, and (G) prevented dextran leakage. MBMECs were transfected by shRNA targeting a scrambled sequence (Sc) or Nrf2. (H) Live/Dead staining with (I) cell counting and (J) LDH assay demonstrated that PC- or 4-HNE-mediated protection was abolished by Nrf2 knockdown. ** and *** $p < 0.01$ and 0.001 *vs* Ctrl; ## and ### $p < 0.01$ and 0.001 *vs* OGD. n.s.: not significant. Scale bar: 50 μm in A and H.

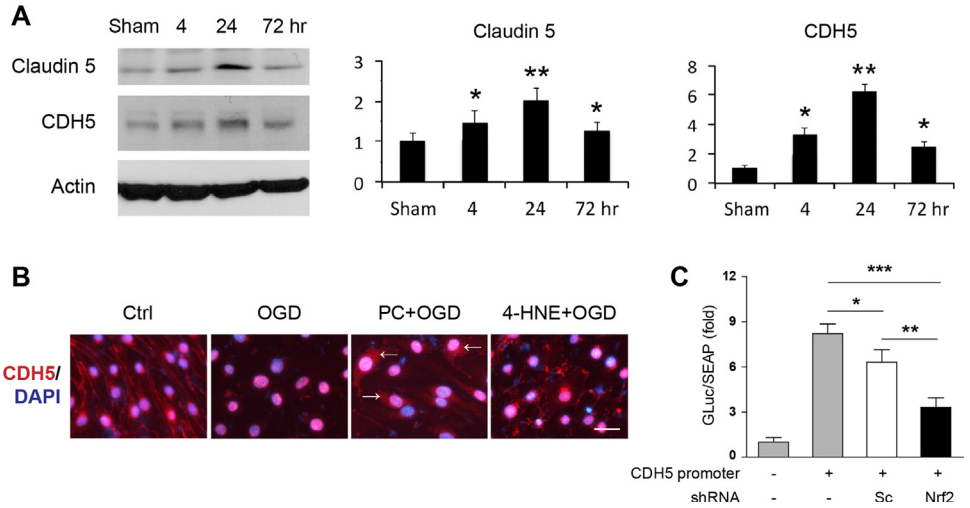

Fig. 6. IPC upregulates junction proteins of the BBB. WT mice were subjected to 12-min IPC. (A) Western blotting and semi-quantitative analyses demonstrated that IPC upregulated claudin-5 and CDH5. n = 3, *p < 0.05 and **p < 0.01 *vs* sham. (B) Consistently in MBMEC cultures, loss of CDH5 was observed in the OGD group, and this effect was partially reversed by both PC and 4-HNE. CDH5-internalization was evident in the PC + OGD group (arrows). Scale bar: 25 μm. (C) A dual-luciferase assay showed significant decreases in CDH5 promoter activity by Nrf2-shRNA, in comparison with Sc-shRNA. *p < 0.05, **p < 0.01, and ***p < 0.001.

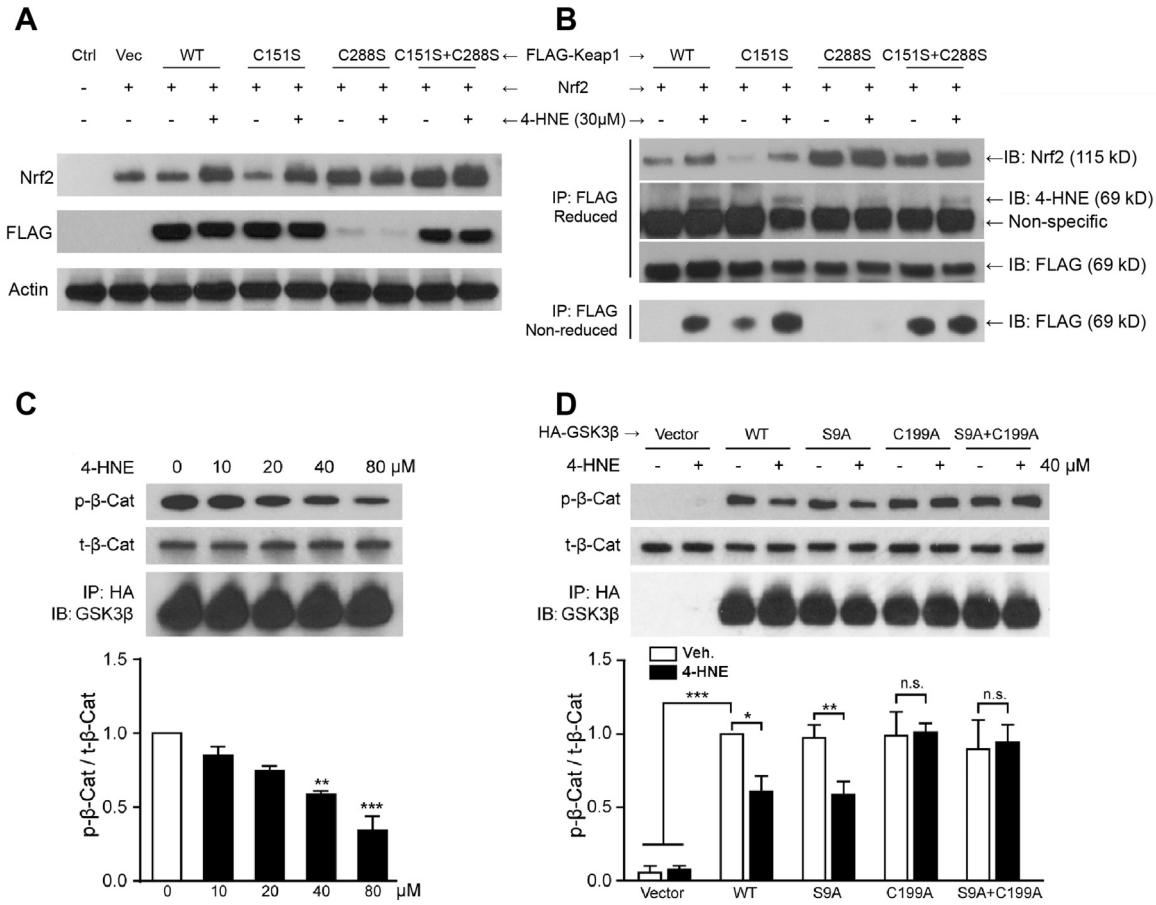

Fig. 7. 4-HNE interrupts the Keap1-Nrf2 interaction through Keap1-C288, and inhibits GSK3β activity by adducting C199. HEK 293T cells were co-transfected with Nrf2 and FLAG-Keap1 (WT and mutant) plasmids, with or without 4-HNE treatment at 30 μM. (A) Western blotting of total cell lysates demonstrates that 4-HNE induced Nrf2 upregulation in both WT and C151S groups, whereas C288S and C151S + C288S groups exhibited high levels of Nrf2 activation regardless of 4-HNE treatment. In addition, a significant decrease in Keap1 is evident in the C288S group. (B) Same amount of FLAG-Keap1 was pulled down with FLAG immunoprecipitation (IP) under either reducing or non-reducing conditions and then subjected to immunoblotting (IB) for Nrf2, 4-HNE, and FLAG. Under non-reducing conditions, 4-HNE failed to increase free unbound C288S-Keap1 and C151S + C288S-Keap1, suggesting C288-dependent 4-HNE inhibition of Keap1-Nrf2 binding. Under reducing conditions, the C288S mutation induced an increase in bound Nrf2, suggesting a key role of C288 in Keap1-Nrf2 disassociation. Immunoblots for 4-HNE indicate that both C151 and C288 can be adducted by 4-HNE. In HEK 293T cells transfected with HA-GSK3β (WT and mutant) plasmids, GSK3β protein was pulled down by HA-resin and subjected to a cell-free GSK3β activity assay. Products in the reaction system were analyzed using Western blotting. (C) 4-HNE inhibited GSK3β activity in a concentration-dependent manner. **p < 0.01, ***p < 0.001 *vs* 0 μM. (D) The activities of both WT and S9A mutant GSK3β were decreased to ~ 60% by 4-HNE, whereas the C199A mutation abrogated the inhibition by 4-HNE. *p < 0.05, **p < 0.01, and ***p < 0.001. n.s.: not significant.

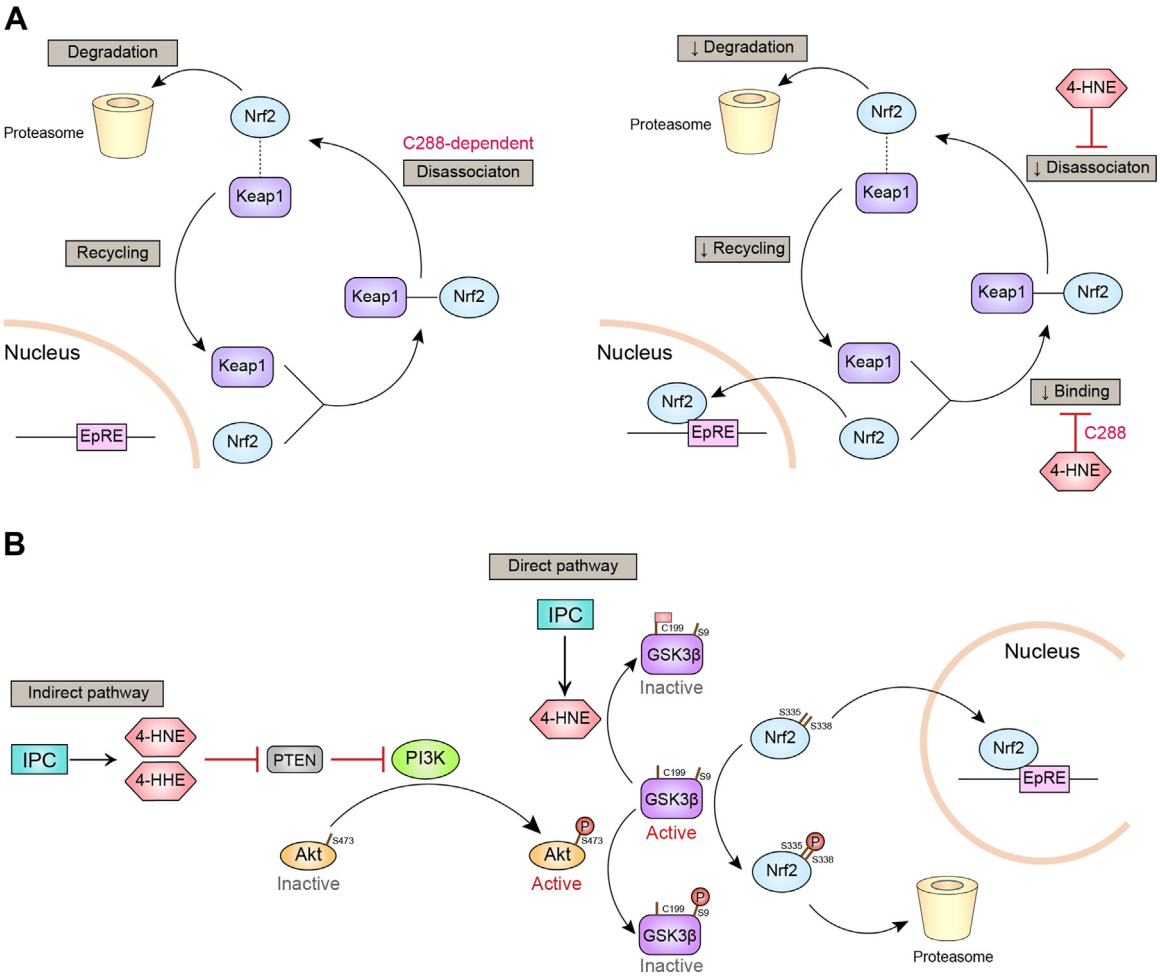

Fig. 8. Diagram showing effects of 4-HNE on Keap1- and GSK3β-mediated Nrf2 degradation. (A) Diagram showing the effects of 4-HNE on the "conforming cycle" in Keap1-mediated Nrf2 degradation. Left panel: under normal conditions, Keap1 binds to Nrf2 and guides it to the proteasome. At the proteasome, Keap1 is dissociated from Nrf2 and is recycled to bind newly synthesized Nrf2. Right panel: we discovered that 4-HNE interrupts both Keap1-Nrf2 binding and their dissociation, leading to a decrease in both Nrf2 degradation and Keap1 recycling; the latter then results in accumulation of newly synthesized Nrf2 which binds EpRE. We also showed that the inhibitory effect of 4-HNE on Keap1-Nrf2 binding is dependent on C288. (B) Diagram showing the effects of 4-HNE on GSK3β-mediated Nrf2 degradation *via* both direct and indirect pathways. In the indirect pathway, both 4-HNE and 4-HHE decrease PTEN activity, which further induces Akt phosphorylation and activation. Activated p-Akt inactivates GSK3β by phosphorylating S9 of GSK3β. We also discovered the direct pathway, in which 4-HNE directly inactivates GSK3β by adducting the C199 residue.

and non-reducing conditions and then subjected to Western blotting. In this assay, free or unbound Keap1 detected under non-reducing conditions indicates Keap1-Nrf2 binding activity (bottom row, Fig. 7B). We observed that 4-HNE reduced binding activities in both WT- and C151S-Keap1, but not in C288S- and C151S + C288S-Keap1, suggesting that 4-HNE disturbs Keap1-Nrf2 binding in a manner that is dependent on the C288 residue (Fig. 8A). On the other hand, non-disassociated Nrf2 arrested by Keap1 was detected under reducing conditions (top row, Fig. 7B). 4-HNE interfered with both WT- and C151S-Keap1 dissociation from Nrf2 (also known as Nrf2 stabilization, Fig. 8A). However, C288-Keap1 exhibited continuous failure of disassociation, regardless of the presence or absence of 4-HNE, suggesting a critical role of the C288 residue in Keap1-Nrf2 disassociation (Fig. 8A). In summary, these findings suggest that C288 is a key residue for Keap1-Nrf2 disassociation under physiological conditions (Fig. 8A); 4-HNE presents inhibitory effects on both binding and disassociation, and the binding inhibition is dependent upon C288 (Fig. 8A).

Next, we detected levels of 4-HNE-modified Keap1 by measuring 4-HNE under reducing conditions, and found a decrease of 4-HNE-modification with C155S and C288S mutations, suggesting that 4-HNE can adduct Keap1 at both C155 and C288 residues, consistent with previous reports [46]. Although our results do not explain the significant decrease in C288S-Keap1 in total cell lysates (Fig. 7A), ubiquitin-mediated degradation may play a role in these effects [22].

3.8. Electrophiles inhibit GSK3β activity in both phosphorylation-dependent and independent manners

Another mechanism of Nrf2 suppression is mediated by the Keap1-independent GSK3β and β-transducin repeated-containing protein (β-TrCP) pathway, in which GSK3β phosphorylates Nrf2, leading to its recognition by β-TrCP and ubiquitin-dependent degradation [8,44]. GSK3β activity can be inhibited by phosphorylation of its S9 residue by Akt [42]. 4-HNE can react with C124 of PTEN and inhibit PTEN activity, leading to increased phosphorylation of Akt and GSK3β in *in vitro* settings [12]. We determined whether IPC also elicited these effects in the mouse brain and whether 4-HHE exhibited similar effects as 4-HNE. Our results showed that 4-HNE increased the phosphorylation of Akt and GSK3β in mouse brains following IPC (Supplementary Fig. 2A), and that both 4-HNE and 4-HHE inhibited PTEN activity, as expected (Supplementary Fig. 2B).

GSK3β and Akt protein kinases require ATP as the donor of the phosphate group. In exploring whether electrophiles can inhibit GSK3β activity in an ATP-competitive fashion, we found that SB216763, an

ATP-competitive GSK3β inhibitor, failed to enhance the HO-1 expression induced by 4-HNE in neurons (Supplementary Fig. 2C). These findings suggest that 4-HNE and SB216763 share a common mechanism in inhibiting GSK3β activity. In recent efforts to develop ATP-competitive GSK3β inhibitors, C199 emerged as an attractive target because it is located at the bottom of the ATP-binding pocket of GSK3β. Thus, the entry of ATP might be blocked when C199 is covalently modified by electrophiles [42]. We therefore hypothesized that lipid electrophiles may inhibit GSK3β by adducting C199, as 4-HNE and 4-HHE react with cysteine and are smaller in size than ATP.

To test the abovementioned hypothesis, we transfected HEK 293T cells with plasmids carrying HA-tagged WT GSK3β or GSK3β with the S9A mutation, C199A mutation, or S9A + C199A double mutation. Proteins were collected by IP with HA-resin and subjected to cell-free GSK3β activity assays [34]. As expected, 4-HNE inhibited WT GSK3β in a concentration-dependent manner (Fig. 7C). In addition, 4-HNE inhibited GSK3β activity in the S9A mutation group, but not in the C199A or S9A + C199A mutation groups (Fig. 7D), indicating the critical role of the C199 site for inhibition of GSK3β by electrophiles. In sum, we have demonstrated two pathways for electrophile inhibition of GSK3β activity—an indirect PTEN/Akt-dependent pathway and a direct C199-dependent pathway (Fig. 8B).

4. Discussion

The present report is the first to suggest that the oxidative stress of IPC may create reactive electrophiles that activate the redox-sensing Nrf2 pathway by adducting C151 and C288 of Keap1 as well as C199 of GSK3β. These electrophile reactions allow Nrf2 to escape Keap1 or GSK3β-dependent degradation and translocate into the nucleus to induce the expression of an array of cytoprotective genes that preserve the BBB and improve neurological outcomes. These findings are consistent with the evolutionarily conserved role of Nrf2 as the master transcription gatekeeper responsible for sensing oxidative injury and maintaining redox equilibrium in injured vertebrate cells [38].

Previous work suggests that rapid IPC only elicits very short-lasting protection against ischemia for up to 3 days [41]. Here, we show that delayed IPC confers protection against stroke in the adult brain for up to 7 days, and, importantly, that the protection is associated with improved sensorimotor functions. Clinical reports show that remote ischemic conditioning of the upper arm in humans leads to beneficial effects for as long as one year when applied twice daily [64]. In the context of the previous literature on repetitive, remote conditioning, our findings suggest that a *single* conditioning episode may exert longer-lasting benefits than expected, which broadens the clinical translatability of conditioning if the ischemic stimulus does not have to be applied every day or twice a day. Our observation that single-episode conditioning effects may last at least one week suggests that future studies in which the frequency, time of day, and duration of conditioning episodes are systematically varied might help optimize the efficacy of conditioning.

Recent studies have shown that HO-1, glutamate-cysteine ligase, and thioredoxins are upregulated after IPC, consistent with the accepted view that delayed IPC requires *de novo* protein synthesis [11]. The expression of these proteins lies under the control of Nrf2 [53,71]. Therefore, we measured Nrf2 levels and EpRE binding activity following IPC and confirmed that IPC induces Nrf2 activation and the transcription and translation of various phase II enzymes. Although neurons, astrocytes, and microvessels all exhibited significant HO-1 induction after 4-HNE stimulation *in vitro*, only microvessels presented with prominent HO-1 expression after IPC *in vivo*, suggesting that the BBB might be an important structure for Nrf2-afforded neuroprotection after IPC. Milder HO-1 expression was observed in astrocytes after IPC, and even less HO-1 expression was observed in neurons. Astrocytic Nrf2 activation has previously been shown to be critical for neuronal survival after stroke [18,31]. It is noteworthy that the HO-1 distribution pattern seen in IPC is quite different from stroke. Previous studies of ours revealed that the highest expression of HO-1 after stroke is not in astrocytes but in Iba-1-positive microglia/macrophages, both in the infarct core and penumbra at 1 and 3 days after stroke [72]. We speculate that these striking differences in cellular HO-1 expression after stroke *vs* IPC reflect differential glial stress responses to varying degrees of oxidative damage and electrophile generation—mildly stressed astrocytes may express Nrf2 to help fortify the BBB, whereas microglia exposed to severe ischemic injury might express HO-1 to aid in the phagocytosis of debris [23].

As expected, IPC provided robust BBB protection in the present study, consistent with previous findings [36,52,70]. The mechanisms underlying IPC-mediated protection of the BBB involve VEGF, ERK, or inflammatory pathways [36,52,70]. We have reported an Nrf2-dependent mechanism underlying BBB protection, as is also the case with BBB protection mediated by sulforaphane, lipopolysaccharide, and hyperbaric oxygen [1,33,55]. Loss of BBB protection is associated with loss of the neuroprotective properties of IPC, consistent with previous studies revealing an indispensable role for Nrf2 [5]. These collective findings also confirm critical role of the BBB in maintaining normal brain function. Not surprisingly, Nrf2 has also been reported to mediate preconditioning with hyperbaric oxygen [68], remote ischemia [7], and inhaled anesthetic gas [67]. Thus, the engagement of the Nrf2 pathway serves as a generalizable and stereotypical mechanism underlying ischemic tolerance against stroke.

Lipid electrophiles are the only category of Nrf2 activators that can be endogenously generated [16] and readily react with cysteines at low concentrations and with histidine and lysine at high concentrations [3,72]. Compared to severe stroke injury, the mild stress of IPC led to the generation of low levels of electrophiles, which are known to play a role in signal transduction cascades. In the present study, mild oxidative stress induced by IPC increased endogenous 4-HNE generation. Furthermore, 4-HNE was shown to directly activate Nrf2 both *in vivo* and *in vitro*, and neutralization of electrophiles abolished IPC-mediated neuroprotection against stroke. These findings validate previous work showing that ischemic tolerance is dependent upon oxidative stress [29,40,43,54].

BBB injury occurs soon after cerebral ischemia [9,51,62], as microvascular ECs are particularly susceptible to oxidative stress and ischemic injury [13]. In the present study, we showed that IPC and 4-HNE treatment protected ECs from loss of integrity and cell death after OGD, consistent with previous reports [2,36]. Furthermore, the Nrf2 knockdown experiments confirmed the essential role of Nrf2 in EC survival and BBB integrity, consistent with previous findings that exogenous Nrf2 inducers such as sulforaphane [74] and curcumin [65] protect the BBB.

TJs and AJs play a critical role in maintaining BBB integrity. In the present study, IPC directly upregulated the TJ protein claudin 5 and the AJ protein CDH5. We previously reported that Nrf2 upregulates claudin 5 [35]; here, we demonstrated that CDH5 may be another new target of Nrf2. These findings support previous reports that Nrf2 knockdown decreased CDH5 expression in human cerebral microvascular EC cultures [47]. We performed a promoter analysis and discovered two EpRE motifs on the mouse CDH5 promoter. The first one is CTGACCAAGCT from aa − 377 to − 366, and the second one is CTGACCAAGCT from aa − 126 to − 115. The calculated binding strength of Nrf2 to the first CDH5 EpRE is 0.29, and to the second one is 0.21 [28]. Our data therefore support our speculation that Nrf2 enhances CDH5 promoter activity, resulting in CDH5 expression and reinforcement of BBB junctions.

Upon exploration of the activation of Nrf2 by electrophiles, we focused on Keap1-dependent Nrf2 degradation, as this pathway is primarily responsible for Nrf2 inactivation [71]. Under normal conditions, Nrf2 is generated constitutively, and Keap1 binds to Nrf2 and guides it to the proteasome for clearance, resulting in a dynamic equilibrium in subthreshold Nrf2 levels. After exposure to electrophiles and other Nrf2

activators, Keap1 undergoes morphologic changes and fails to encourage Nrf2 degradation, leading indirectly to Nrf2 translocation to the nucleus. According to the "conformation cycling" theory [4] (Fig. 8A), Keap1 disassociates from Nrf2 after guiding Nrf2 to the proteasome, recycles to the cytosol, and binds newly-synthesized Nrf2. Electrophiles disrupt the disassociation and recycling of Keap1, resulting in accumulation and activation of newly-synthesized Nrf2. The most important stress sensors in Keap1 are C151 in the Bric-a-Brac (BTB) domain and C288 in the redox sensitive intervening region (IVR) domain. Therefore, we explored the effect of 4-HNE on Keap1-Nrf2 binding and disassociation using WT and point-mutant Keap1. We discovered that the C288S mutation led to chronic Nrf2 activation, in agreement with previous reports that C288S disables Keap1-Nrf2 association (Fig. 8A) [32,63]. Our data also supported the "conformation cycling" theory [4] by verifying 4-HNE-mediated disturbance of disassociation. We confirmed that both C155 and C288 could be adducted by 4-HNE [46] by verifying decreased 4-HNE modification under mutant conditions. Most importantly, 4-HNE decreased Keap1 binding activity in WT and C151S mutants, an effect that was absent in C288S and C151S + C288S double mutants, suggesting a critical role of the C288 residue in 4-HNE-mediated decreases in Keap1-Nrf2 binding (Fig. 8A). To the best of our knowledge, we are the first to report the phenomenon that 4-HNE can disturb Keap1-Nrf2 binding through the C288 residue of Keap1.

The GSK3β/β-TrCP pathway is responsible for Nrf2 degradation in a Keap1-independent manner. GSK3β phosphorylates the Neh6 domain of Nrf2 at S342, S347, S335, and S338 [48,71]; the phosphorylated Nrf2 is then recognized by β-TrCP, an E3 ubiquitin ligase, and subjected to ubiquitination and degradation. It is not clear whether and how electrophiles influence GSK3β activity. Unlike most other cellular kinases that are normally inactive, GSK3β is active under resting conditions and continuously phosphorylates Nrf2, leading to its constitutive degradation. Several GSK3β inhibitory signals have been reported, including phosphoinositide 3-kinase (PI3K)/Akt, mechanistic target of rapamycin (mTOR)/P70, Ras/P90, P38/mitogen-activated protein kinase (MAPK), and protein kinase C (PKC). Among these inhibitory signals, the most well-established is the PI3K/Akt signaling pathway [19]. Specifically, PI3K activates Akt through phosphorylation of its S473 residue; p-Akt (S473) consequently phosphorylates GSK3β at the S9 residue, leading to its inactivation [12,42] (Fig. 8B). Akt phosphorylation by PI3K can be inhibited by PTEN, and 4-HNE has been shown to inhibit PTEN activity [12]. Our findings support previous findings and confirm that both 4-HNE and 4-HHE decrease PTEN activity. Similar results were reported in WT and Keap1$^{-/-}$ mouse embryonic fibroblasts treated with the electrophile tert-butylhydroquinone [19].

There are no previous reports of an interaction between GSK3β and Nrf2 in IPC. We found that lipid electrophiles inhibited GSK3β activity through both indirect (PTEN and Akt) and direct (C199) mechanisms. The finding that 4-HNE can directly inhibit GSK3β activity *via* C199 was made in a cell-free system without potential interference from other molecules. Perez et al. suggested that GSK3β-C199 might be a potential target for novel GSK3β inhibitors, because C199 is at the bottom of the ATP-binding domain [42]. We established a mechanism in which 4-HNE directly adducts the ATP entrance site of GSK3β-C199, thereby inhibiting GSK3β kinase activity. This overall effect of GSK3β inhibition further facilitates activation of Nrf2 in IPC.

HEK 293 and HEK 293T are modified cell lines widely used in the field of molecular biology, especially in studies of protein-protein interactions [22,30,32]. Although our data revealed the molecular mechanisms by which 4-HNE activates Nrf2 in a live cellular system, it remains to be confirmed that this mechanism also operates in the confines of the BBB and further studies using primary endothelial cells are warranted.

In conclusion, we report here relatively long-lasting protective effects of IPC-mediated ischemic tolerance in the BBB and the parenchyma of the brain, and demonstrate a novel biological mechanism underlying activation of the master transcription factor Nrf2. IPC leads to release of lipid electrophiles, such as 4-HNE and 4-HHE, which activate the Nrf2 pathway and induce translation of endogenous cytoprotective enzymes and BBB junction proteins. We report two independent mechanisms whereby lipid electrophiles activate Nrf2: [1] adduction of Keap1 to release Nrf2 from constitutive degradation, [2] inactivation of GSK3β through inhibition of PTEN activity or adduction of the C199 residue of GSK3β, and hindrance of ATP entry into its binding pocket. We conclude that Nrf2 is a promising therapeutic target to protect the mammalian brain against stroke.

Acknowledgements

This work was supported by grants from the US National Institutes of Health (NS092810 to FZ; NS089534, NS095671, NS105430 and NS036736 to JC), US Department of Veterans Affairs (BX002495 to JC), the American Heart Association (10SDG2560122 to FZ), and the National Natural Science Foundation of China (81271276 to FZ; 81228008 to JC). We thank Pat Strickler for administrative support.

Author contributions

J.C. and F.Z. designed and supervised the project. T.Y., M.Z., S.W., and L.Z. performed in vitro experiments. Y.Sun, M.L., Q.L. and F.Z. performed in vivo experiments. T.Y. and F.Z. wrote the manuscript. Y.Shi, R.K.L., and J.C. helped with the editing of the manuscript.

Competing financial interests

None.

Appendix A. Supplementary material

Supplementary data associated with this article can be found in the online version at http://dx.doi.org/10.1016/j.redox.2018.05.001.

References

[1] A. Alfieri, S. Srivastava, R.C. Siow, D. Cash, M. Modo, M.R. Duchen, P.A. Fraser, S.C. Williams, G.E. Mann, Sulforaphane preconditioning of the Nrf2/HO-1 defense pathway protects the cerebral vasculature against blood-brain barrier disruption and neurological deficits in stroke, Free Radic. Biol. Med. 65 (2013) 1012–1022.
[2] A.V. Andjelkovic, S.M. Stamatovic, R.F. Keep, The protective effects of preconditioning on cerebral endothelial cells in vitro, J. Cereb. Blood Flow Metab. 23 (2003) 1348–1355.
[3] L. Baird, A.T. Dinkova-Kostova, The cytoprotective role of the Keap1-Nrf2 pathway, Arch. Toxicol. 85 (2011) 241–272.
[4] L. Baird, D. Lleres, S. Swift, A.T. Dinkova-Kostova, Regulatory flexibility in the Nrf2-mediated stress response is conferred by conformational cycling of the Keap1-Nrf2 protein complex, Proc. Natl. Acad. Sci. USA 110 (2013) 15259–15264.
[5] K.F. Bell, B. Al-Mubarak, J.H. Fowler, P.S. Baxter, K. Gupta, T. Tsujita, S. Chowdhry, R. Patani, S. Chandran, K. Horsburgh, J.D. Hayes, G.E. Hardingham, Mild oxidative stress activates Nrf2 in astrocytes, which contributes to neuroprotective ischemic preconditioning, Proc. Natl. Acad. Sci. USA 108 (E1–2) (2011) (author reply E3–4).
[6] V. Bouet, M. Boulouard, J. Toutain, D. Divoux, M. Bernaudin, P. Schumann-Bard, T. Freret, The adhesive removal test: a sensitive method to assess sensorimotor deficits in mice, Nat. Protoc. 4 (2009) 1560–1564.
[7] M. Chen, M. Zhang, X. Zhang, J. Li, Y. Wang, Y. Fan, R. Shi, Limb ischemic preconditioning protects endothelium from oxidative stress by enhancing nrf2 translocation and upregulating expression of antioxidases, PLoS One 10 (2015) e0128455.
[8] A. Cuadrado, Structural and functional characterization of Nrf2 degradation by glycogen synthase kinase 3/beta-TrCP, Free Radic. Biol. Med. 88 (2015) 147–157.
[9] G.J. del Zoppo, T. Mabuchi, Cerebral microvessel responses to focal ischemia, J. Cereb. Blood Flow Metab. 23 (2003) 879–894.
[10] B.M. Demaerschalk, H.M. Hwang, G. Leung, Cost analysis review of stroke centers, telestroke, and rt-PA, Am. J. Manag. Care 16 (2010) 537–544.
[11] V.K. Dhodda, K.A. Sailor, K.K. Bowen, R. Vemuganti, Putative endogenous mediators of preconditioning-induced ischemic tolerance in rat brain identified by genomic and proteomic analysis, J. Neurochem. 89 (2004) 73–89.
[12] B. Dozza, M.A. Smith, G. Perry, M. Tabaton, P. Strocchi, Regulation of glycogen synthase kinase-3β by products of lipid peroxidation in human neuroblastoma cells, J. Neurochem. 89 (2004) 1224–1232.

[13] L.R. Freeman, J.N. Keller, Oxidative stress and cerebral endothelial cells: regulation of the blood-brain-barrier and antioxidant based interventions, Biochim. Biophys. Acta 1822 (2012) 822–829.
[14] J.M. Gidday, Cerebral preconditioning and ischaemic tolerance, Nat. Rev. Neurosci. 7 (2006) 437–448.
[15] S. Gory, M. Vernet, M. Laurent, E. Dejana, J. Dalmon, P. Huber, The vascular endothelial-cadherin promoter directs endothelial-specific expression in transgenic mice, Blood 93 (1999) 184–192.
[16] M. Guichardant, B. Chantegrel, C. Deshayes, A. Doutheau, P. Moliere, M. Lagarde, Specific markers of lipid peroxidation issued from n-3 and n-6 fatty acids, Biochem. Soc. Trans. 32 (2004) 139–140.
[17] A. Hartsock, W.J. Nelson, Adherens and tight junctions: structure, function and connections to the actin cytoskeleton, Biochim. Biophys. Acta 1778 (2008) 660–669.
[18] R.E. Haskew-Layton, J.B. Payappilly, N.A. Smirnova, T.C. Ma, K.K. Chan, T.H. Murphy, H. Guo, B. Langley, R. Sultana, D.A. Butterfield, S. Santagata, M.J. Alldred, I.G. Gazaryan, G.W. Bell, S.D. Ginsberg, R.R. Ratan, Controlled enzymatic production of astrocytic hydrogen peroxide protects neurons from oxidative stress via an Nrf2-independent pathway, Proc. Natl. Acad. Sci. USA 107 (2010) 17385–17390.
[19] J.D. Hayes, S. Chowdhry, A.T. Dinkova-Kostova, C. Sutherland, Dual regulation of transcription factor Nrf2 by Keap1 and by the combined actions of beta-TrCP and GSK-3, Biochem. Soc. Trans. 43 (2015) 611–620.
[20] J.D. Hayes, M. McMahon, Molecular basis for the contribution of the antioxidant responsive element to cancer chemoprevention, Cancer Lett. 174 (2001) 103–113.
[21] W.D. Holtzclaw, A.T. Dinkova-Kostova, P. Talalay, Protection against electrophile and oxidative stress by induction of phase 2 genes: the quest for the elusive sensor that responds to inducers, Adv. Enzym. Regul. 44 (2004) 335–367.
[22] F. Hong, K.R. Sekhar, M.L. Freeman, D.C. Liebler, Specific patterns of electrophile adduction trigger Keap1 ubiquitination and Nrf2 activation, J. Biol. Chem. 280 (2005) 31768–31775.
[23] C. Hualin, X. Wenli, L. Dapeng, L. Xijing, P. Xiuhua, P. Qingfeng, The anti-inflammatory mechanism of heme oxygenase-1 induced by hemin in primary rat alveolar macrophages, Inflammation 35 (2012) 1087–1093.
[24] P. Huber, J. Dalmon, J. Engiles, F. Breviario, S. Gory, L.D. Siracusa, A.M. Buchberg, E. Dejana, Genomic structure and chromosomal mapping of the mouse VE-cadherin gene (Cdh5), Genomics 32 (1996) 21–28.
[25] K. Itoh, T. Chiba, S. Takahashi, T. Ishii, K. Igarashi, Y. Katoh, T. Oyake, N. Hayashi, K. Satoh, I. Hatayama, M. Yamamoto, Y.-i. Nabeshima, An Nrf2/small Maf heterodimer mediates the induction of phase II detoxifying enzyme genes through antioxidant response elements, Biochem. Biophys. Res. Commun. 236 (1997) 313–322.
[26] K. Itoh, N. Wakabayashi, Y. Katoh, T. Ishii, K. Igarashi, J.D. Engel, M. Yamamoto, Keap1 represses nuclear activation of antioxidant responsive elements by Nrf2 through binding to the amino-terminal Neh2 domain, Genes Dev. 13 (1999) 76–86.
[27] K. Kitagawa, M. Matsumoto, M. Tagaya, R. Hata, H. Ueda, M. Niinobe, N. Handa, R. Fukunaga, K. Kimura, K. Mikoshiba, et al., 'Ischemic tolerance' phenomenon found in the brain, Brain Res. 528 (1990) 21–24.
[28] S.M. Kuosmanen, S. Viitala, T. Laitinen, M. Perakyla, P. Polonen, E. Kansanen, H. Leinonen, S. Raju, A. Wienecke-Baldacchino, A. Narvanen, A. Poso, M. Heinaniemi, S. Heikkinen, A.L. Levonen, The effects of sequence variation on genome-wide NRF2 binding–new target genes and regulatory SNPs, Nucleic Acids Res. 44 (2016) 1760–1775.
[29] A. Landar, J.W. Zmijewski, D.A. Dickinson, C. Le Goffe, M.S. Johnson, G.L. Milne, G. Zanoni, G. Vidari, J.D. Morrow, V.M. Darley-Usmar, Interaction of electrophilic lipid oxidation products with mitochondria in endothelial cells and formation of reactive oxygen species, Am. J. Physiol. Heart Circ. Physiol. 290 (2006) H1777–H1787.
[30] A. Lau, X.J. Wang, F. Zhao, N.F. Villeneuve, T. Wu, T. Jiang, Z. Sun, E. White, D.D. Zhang, A noncanonical mechanism of Nrf2 activation by autophagy deficiency: direct interaction between Keap1 and p62, Mol. Cell. Biol. 30 (2010) 3275–3285.
[31] J.M. Lee, M.J. Calkins, K. Chan, Y.W. Kan, J.A. Johnson, Identification of the NF-E2-related factor-2-dependent genes conferring protection against oxidative stress in primary cortical astrocytes using oligonucleotide microarray analysis, J. Biol. Chem. 278 (2003) 12029–12038.
[32] A.L. Levonen, A. Landar, A. Ramachandran, E.K. Ceaser, D.A. Dickinson, G. Zanoni, J.D. Morrow, V.M. Darley-Usmar, Cellular mechanisms of redox cell signalling: role of cysteine modification in controlling antioxidant defences in response to electrophilic lipid oxidation products, Biochem. J. 378 (2004) 373–382.
[33] W.C. Li, D.M. Jiang, N. Hu, X.T. Qi, B. Qiao, X.J. Luo, Lipopolysaccharide preconditioning attenuates neuroapoptosis and improves functional recovery through activation of Nrf2 in traumatic spinal cord injury rats, Int. J. Neurosci. 123 (2013) 240–247.
[34] W. Mai, K. Miyashita, A. Shakoori, B. Zhang, Z.W. Yu, Y. Takahashi, Y. Motoo, K. Kawakami, T. Minamoto, Detection of active fraction of glycogen synthase kinase 3beta in cancer cells by nonradioisotopic in vitro kinase assay, Oncology 71 (2006) 297–305.
[35] L. Mao, T. Yang, X. Li, X. Lei, Y. Sun, Y. Zhao, W. Zhang, Y. Gao, B. Sun, F. Zhang, Protective effects of sulforaphane in experimental vascular cognitive impairment: contribution of the Nrf2 pathway, J. Cereb. Blood Flow Metab. (2018) (271678X18764083).
[36] T. Masada, Y. Hua, G. Xi, S.R. Ennis, R.F. Keep, Attenuation of ischemic brain edema and cerebrovascular injury after ischemic preconditioning in the rat, J. Cereb. Blood Flow Metab. 21 (2001) 22–33.
[37] M.A. Moskowitz, E.H. Lo, C. Iadecola, The science of stroke: mechanisms in search of treatments, Neuron 67 (2010) 181–198.
[38] K. Mukaigasa, L.T. Nguyen, L. Li, H. Nakajima, M. Yamamoto, M. Kobayashi, Genetic evidence of an evolutionarily conserved role for Nrf2 in the protection against oxidative stress, Mol. Cell. Biol. 32 (2012) 4455–4461.
[39] S.V. Narayanan, K.R. Dave, M.A. Perez-Pinzon, Ischemic preconditioning and clinical scenarios, Curr. Opin. Neurol. 26 (2013) 1–7.
[40] T. Ohtsuki, M. Matsumoto, K. Kuwabara, K. Kitagawa, K. Suzuki, N. Taniguchi, T. Kamada, Influence of oxidative stress on induced tolerance to ischemia in gerbil hippocampal neurons, Brain Res. 599 (1992) 246–252.
[41] M.A. Perez-Pinzon, G.P. Xu, W.D. Dietrich, M. Rosenthal, T.J. Sick, Rapid preconditioning protects rats against ischemic neuronal damage after 3 but not 7 days of reperfusion following global cerebral ischemia, J. Cereb. Blood Flow Metab. 17 (1997) 175–182.
[42] D.I. Perez, V. Palomo, C. Perez, C. Gil, P.D. Dans, F.J. Luque, S. Conde, A. Martinez, Switching reversibility to irreversibility in glycogen synthase kinase 3 inhibitors: clues for specific design of new compounds, J. Med. Chem. 54 (2011) 4042–4056.
[43] F. Puisieux, D. Deplanque, H. Bulckaen, P. Maboudou, P. Gele, M. Lhermitte, G. Lebuffe, R. Bordet, Brain ischemic preconditioning is abolished by antioxidant drugs but does not up-regulate superoxide dismutase and glutathione peroxidase, Brain Res. 1027 (2004) 30–37.
[44] P. Rada, A.I. Rojo, N. Evrard-Todeschi, N.G. Innamorato, A. Cotte, T. Jaworski, J.C. Tobon-Velasco, H. Devijver, M.F. Garcia-Mayoral, F. Van Leuven, J.D. Hayes, G. Bertho, A. Cuadrado, Structural and functional characterization of Nrf2 degradation by the glycogen synthase kinase 3/beta-TrCP axis, Mol. Cell. Biol. 32 (2012) 3486–3499.
[45] T.K. Rudolph, B.A. Freeman, Transduction of redox signaling by electrophile-protein reactions, Sci. Signal. 2 (2009) (re7-).
[46] R. Saito, T. Suzuki, K. Hiramoto, S. Asami, E. Naganuma, H. Suda, T. Iso, H. Yamamoto, M. Morita, L. Baird, Y. Furusawa, T. Negishi, M. Ichinose, M. Yamamoto, Characterizations of three major cysteine sensors of Keap1 in stress response, Mol. Cell. Biol. 36 (2015) 271–284.
[47] R.K. Sajja, K.N. Green, L. Cucullo, Altered Nrf2 signaling mediates hypoglycemia-induced blood-brain barrier endothelial dysfunction in vitro, PLoS One 10 (2015) e0122358.
[48] M. Salazar, A.I. Rojo, D. Velasco, R.M. de Sagarra, A. Cuadrado, Glycogen synthase kinase-3beta inhibits the xenobiotic and antioxidant cell response by direct phosphorylation and nuclear exclusion of the transcription factor Nrf2, J. Biol. Chem. 281 (2006) 14841–14851.
[49] S. Schildge, C. Bohrer, K. Beck, C. Schachtrup, Isolation and culture of mouse cortical astrocytes, J. Vis. Exp. (2013).
[50] C.T. Shearn, R.L. Smathers, B.J. Stewart, K.S. Fritz, J.J. Galligan, N. Hail Jr., D.R. Petersen, Phosphatase and tensin homolog deleted on chromosome 10 (PTEN) inhibition by 4-hydroxynonenal leads to increased Akt activation in hepatocytes, Mol. Pharmacol. 79 (2011) 941–952.
[51] Y. Shi, L. Zhang, H. Pu, L. Mao, X. Hu, X. Jiang, N. Xu, R.A. Stetler, F. Zhang, X. Liu, R.K. Leak, R.F. Keep, X. Ji, J. Chen, Rapid endothelial cytoskeletal reorganization enables early blood-brain barrier disruption and long-term ischaemic reperfusion brain injury, Nat. Commun. 7 (2016) 10523.
[52] J.A. Shin, Y.A. Kim, S.I. Jeong, K.E. Lee, H.S. Kim, E.M. Park, Extracellular signal-regulated kinase1/2-dependent changes in tight junctions after ischemic preconditioning contributes to tolerance induction after ischemic stroke, Brain Struct. Funct. 220 (2015) 13–26.
[53] A.A. Shokeir, A.M. Hussein, N. Barakat, A. Abdelaziz, M. Elgarba, A. Awadalla, Activation of nuclear factor erythroid 2-related factor 2 (Nrf2) and Nrf-2-dependent genes by ischaemic pre-conditioning and post-conditioning: new adaptive endogenous protective responses against renal ischaemia/reperfusion injury, Acta Physiol. 210 (2014) 342–353.
[54] M. Simerabet, E. Robin, I. Aristi, S. Adamczyk, B. Tavernier, B. Vallet, R. Bordet, G. Lebuffe, Preconditioning by an in situ administration of hydrogen peroxide: involvement of reactive oxygen species and mitochondrial ATP-dependent potassium channel in a cerebral ischemia-reperfusion model, Brain Res. 1240 (2008) 177–184.
[55] Y. Soejima, R.P. Ostrowski, A. Manaenko, M. Fujii, J. Tang, J.H. Zhang, Hyperbaric oxygen preconditioning attenuates hyperglycemia enhanced hemorrhagic transformation after transient MCAO in rats, Med. Gas Res. 2 (2012) 9.
[56] R.A. Stetler, G. Cao, Y. Gao, F. Zhang, S. Wang, Z. Weng, P. Vosler, L. Zhang, A. Signore, S.H. Graham, J. Chen, Hsp27 protects against ischemic brain injury via attenuation of a novel stress-response cascade upstream of mitochondrial cell death signaling, J. Neurosci. 28 (2008) 13038–13055.
[57] R.A. Stetler, Y. Gao, R.K. Leak, Z. Weng, Y. Shi, L. Zhang, H. Pu, F. Zhang, X. Hu, S. Hassan, C. Ferguson, G.E. Homanics, G. Cao, M.V. Bennett, J. Chen, APE1/Ref-1 facilitates recovery of gray and white matter and neurological function after mild stroke injury, Proc. Natl. Acad. Sci. USA 113 (2016) E3558–E3567.
[58] R.A. Stetler, R.K. Leak, Y. Gan, P. Li, F. Zhang, X. Hu, Z. Jing, J. Chen, M.J. Zigmond, Y. Gao, Preconditioning provides neuroprotection in models of CNS disease: paradigms and clinical significance, Prog. Neurobiol. 114 (2014) 58–83.
[59] S.L. Stevens, P.Y. Leung, K.B. Vartanian, B. Gopalan, T. Yang, R.P. Simon, M.P. Stenzel-Poore, Multiple preconditioning paradigms converge on interferon regulatory factor-dependent signaling to promote tolerance to ischemic brain injury, J. Neurosci. 31 (2011) 8456–8463.
[60] A.M. Stowe, T. Altay, A.B. Freie, J.M. Gidday, Repetitive hypoxia extends endogenous neurovascular protection for stroke, Ann. Neurol. 69 (2011) 975–985.
[61] B.A. Tannous, Gaussia luciferase reporter assay for monitoring biological processes in culture and in vivo, Nat. Protoc. 4 (2009) 582–591.
[62] B.K. Wacker, A.B. Freie, J.L. Perfater, J.M. Gidday, Junctional protein regulation by sphingosine kinase 2 contributes to blood-brain barrier protection in hypoxic preconditioning-induced cerebral ischemic tolerance, J. Cereb. Blood Flow Metab. 32 (2012) 1014–1023.

[63] N. Wakabayashi, A.T. Dinkova-Kostova, W.D. Holtzclaw, M.I. Kang, A. Kobayashi, M. Yamamoto, T.W. Kensler, P. Talalay, Protection against electrophile and oxidant stress by induction of the phase 2 response: fate of cysteines of the Keap1 sensor modified by inducers, Proc. Natl. Acad. Sci. USA 101 (2004) 2040–2045.
[64] Y. Wang, R. Meng, H. Song, G. Liu, Y. Hua, D. Cui, L. Zheng, W. Feng, D.S. Liebeskind, M. Fisher, X. Ji, Remote ischemic conditioning may improve outcomes of patients with cerebral small-vessel disease, Stroke 48 (2017) 3064–3072.
[65] Y.F. Wang, Y.T. Gu, G.H. Qin, L. Zhong, Y.N. Meng, Curcumin ameliorates the permeability of the blood-brain barrier during hypoxia by upregulating heme oxygenase-1 expression in brain microvascular endothelial cells, J. Mol. Neurosci. 51 (2013) 344–351.
[66] W.W. Wasserman, W.E. Fahl, Functional antioxidant responsive elements, Proc. Natl. Acad. Sci. USA 94 (1997) 5361–5366.
[67] T. Yang, Y. Sun, F. Zhang, Anti-oxidative aspect of inhaled anesthetic gases against acute brain injury, Med. Gas Res. 6 (2016) 223–226.
[68] X. Zhai, H. Lin, Y. Chen, X. Chen, J. Shi, O. Chen, J. Li, X. Sun, Hyperbaric oxygen preconditioning ameliorates hypoxia-ischemia brain damage by activating Nrf2 expression in vivo and in vitro, Free Radic. Res. 50 (2016) 454–466.
[69] F. Zhang, S. Wang, M. Zhang, Z. Weng, P. Li, Y. Gan, L. Zhang, G. Cao, Y. Gao, R.K. Leak, M.B. Sporn, J. Chen, Pharmacological induction of heme oxygenase-1 by a triterpenoid protects neurons against ischemic injury, Stroke 43 (2012) 1390–1397.
[70] F.Y. Zhang, X.C. Chen, H.M. Ren, W.M. Bao, Effects of ischemic preconditioning on blood-brain barrier permeability and MMP-9 expression of ischemic brain, Neurol. Res. 28 (2006) 21–24.
[71] M. Zhang, C. An, Y. Gao, R.K. Leak, J. Chen, F. Zhang, Emerging roles of Nrf2 and phase II antioxidant enzymes in neuroprotection, Prog. Neurobiol. 100 (2013) 30–47.
[72] M. Zhang, S. Wang, L. Mao, R.K. Leak, Y. Shi, W. Zhang, X. Hu, B. Sun, G. Cao, Y. Gao, Y. Xu, J. Chen, F. Zhang, Omega-3 fatty acids protect the brain against ischemic injury by activating Nrf2 and upregulating heme oxygenase 1, J. Neurosci. 34 (2014) 1903–1915.
[73] W. Zhang, X. Hu, W. Yang, Y. Gao, J. Chen, Omega-3 polyunsaturated fatty acid supplementation confers long-term neuroprotection against neonatal hypoxic–ischemic brain injury through anti-inflammatory actions, Stroke 41 (2010) 2341–2347.
[74] J. Zhao, A.N. Moore, J.B. Redell, P.K. Dash, Enhancing expression of Nrf2-driven genes protects the blood brain barrier after brain injury, J. Neurosci. 27 (2007) 10240–10248.